Evaluation of
Normal Tissue Complication Probability
and Risk of Second Primary Cancer
in Prostate Radiotherapy

Rungdham Takam

Thesis submitted for the degree of

Doctor of Philosophy

in

The School of Chemistry and Physics,

The University of Adelaide

Supervisors

A/Prof. Eva Bezak

Prof. Eric E. Yeoh

Dr. Guilin Liu

THE UNIVERSITY
OF ADELAIDE
AUSTRALIA

April 2010

Chapter 5

Second primary cancer associated with prostate cancer radiotherapy

5.1 Introduction

As previously discussed in chapters 3 and 4, normal tissue complications (toxicities) arise following radiation therapy of prostate cancer. The complications which occur within a short period (≤3 months) after completion of radiation treatment are characterized as acute normal tissue complications or early toxicities. Normal tissue complications may however arise many (>3) months or years after completion of the treatment. In the extreme, these late normal tissue complications include the risk of developing radiation-induced second primary cancer (SPC). This has been increasingly observed in patients treated with

radiation therapy. Longer survival times for patients with cancer as a result of improvements in radiation therapy techniques and earlier diagnosis at younger ages contribute to an increased risk of radiation-induced carcinogenesis (Brenner *et al* 2000). In general, second primary cancer is defined as a new tumor (neoplasm) which develops from normal tissue exposed to radiation and has histopathologic features different from the primary tumor ≥5 years after radiation treatment (Abdel-Wahab *et al* 2008).

The increased success of radiotherapy (alone or in the combination with other treatment modalities) has led to an increase in life expectancy of patients with prostate cancer many of whom are cured of their disease (Dasu & Toma-Dasu 2005) and therefore at the risk of development of a second primary cancer (Dorr & Herrmann 2008). This is because the latent period between radiation exposure and the development of SPC is 5 to 15 years which may be perceived as a negative long term consequence of the successful radiation therapy for prostate cancer (Baxter *et al* 2005).

In the United States, the 5-year relative survival rate of locally and regionally confined prostate cancer approaches 100% and the 5-year survival rate for all stages of prostate cancer combined has increased from 69% to almost 99% over the past 25 years (American Cancer Society 2008). The most recent data of 10-year relative survival of 91% and of 15-year relative survival of 76% has also been reported to result from earlier diagnosis and improved treatments. Hence, there is distinct chance of the development of SPC among these long-term prostate cancer survivors after radiation therapy. However, the influence of radiation technique on the risk of development of SPC has not been adequately studied (Abdel-Wahab *et*

al 2008). The need to compare radiotherapy plans in order to reduce if not avoid SPC induction is likely to increase in the future (Schneider *et al* 2005). Therefore, in this chapter, the risk of second malignancy following various radiation treatment techniques for localized prostate cancer is examined and discussed.

5.2 Evaluations of the second primary cancer risk

Generally, there are two main approaches to evaluate the risk of second primary cancers: an epidemiologic study and model-based risk estimation. In the first approach, two classic epidemiologic study designs using cohort and case-control methodologies have been used in most studies of therapy-related cancers (Travis 2006). Details of this approach will not be discussed in this thesis but the results of various epidemiologic studies of second primary cancers after prostate cancer irradiation will be presented in this chapter in support of the model used in risk estimation.

5.2.1 Epidemiologic studies on incidence of second primary cancers following prostate cancer radiotherapy

Two groups of epidemiologic study results are discussed in this section: a) single institutional studies, b) large cohorts studies. The reports are presented in a chronological order.

Apart from the increased risk of bladder second primary cancer reported in a few studies (Neugut *et al* 1997, Pawlish *et al* 1997, Movsas *et al* 1998, and Brenner *et al* 2000), most single institutional studies suggest that the risk of SPCs is less than that expected from the general population of patients with prostate cancer (Kleinerman *et al* 1985 and Osterlind *et al* 1985). These studies may have some

methodological flaws which are pointed out in the discussion below. This is highlighted by the study of Abdel-Wahab *et al* (2008) which involved large patient numbers (228,235 patients) with long follow-up (median of 6 – 8 years) and better surveillance after completion of radiotherapy that suggests that there is an increase in the risk of SPCs associated with prostate cancer radiotherapy particularly in External Beam Radiotherapy (EBRT).

For the single institution studies, a series of epidemiologic study reports related to the incidence of SPCs involving a large number of patients following prostate cancer therapy over considerably long periods (several decades in some studies) of follow-up provide the baseline data for comparisons of the incidence of new neoplasms between various forms of treatment. For example, in the study to evaluate the risk of second malignancy reported by Kleinerman *et al* (1985), 18,315 men with cancers of the prostate or testis registered in the Connecticut Tumor Registry in Connecticut during 1935 and 1982 were involved. Among these patients, 1,053 second primary cancers developed compared with the 1,241 expected based on rates in the general population resulting in a Relative Risk (RR) of 0.85. This figure, hence, suggested a significant reduction in the risk of SPC following any type of prostate cancer treatment (including radiotherapy) relative to the general population. Among men under 65 years of age this risk was equal to that expected (RR = 1.0). The reduction in the SPC risk among men of 65 years of age and older may be attributable to under-investigation for this elderly often unfit sub-group of patients. Reductions of SPC in lung and digestive tract including esophagus, stomach and colon were observed. In contrast, the increase in the risk of SPC of the salivary glands (RR = 2.7) was observed. Although no information

related to prostate treatment modality was provided in this study, most of the prostate patients involved in this report were stated to have prostatectomy as their major treatment and this may be associated with the deficit of second malignancies in this study.

In Denmark, 19,886 men with prostate cancer during 1943 – 1980 were evaluated for the incidence of SPCs (Osterlind *et al* 1985). Among the study population, 11% received radiotherapy of unspecified technique either alone or in combination with surgery and other treatment, 28% were treated with surgery alone, and 35% received other treatments. Of the 19,886 men, 594 (3.0%) developed second primary cancer compared to the 1,176 expected on the basis of rates in the general population resulting in RR of 0.51 in the study population. Similarly to the report of Kleinerman *et al* (1985) described above, the reduced risk of second primary cancer was observed for cancers of digestive organs and respiratory system. However, unlike the previous report, there was not one site with an increased risk of SPC. The reduced risk of SPC was also attributed to under-reporting as a result of lack of diagnostic investigation of the population of elderly patients.

From these two reports, the incidence of second malignancies after different interventions for prostate cancer was lower than that expected from rates in the general population although only a minority of the patient population received radiation therapy.

The one report of the SPC incidence following the diagnosis and treatment of primary invasive cancers of renal parenchyma and pelvis or prostate in Australia was based on the work of McCredie *et al* (1996). Using the data from the New South Wales Central Cancer Registry for the period 1972 – 1991, the 23,067 men

diagnosed with prostatic cancer were the subjects of their study. The average age when prostate cancer was diagnosed was 73 years and the total number of patients who developed SPCs was 1,096 (RR = 0.79). The observed number of SPCs for most sites was lower than expected, particularly for stomach, pancreas, and lung. Although, the risk of kidney second cancer bordered on being significantly increased (RR = 1.3), i.e. was considered to be associated with estrogen treatment for prostate cancer. The reduced risk of SPCs among the elderly population of patients was also attributed to less medical surveillance and diagnostic intervention although similar to the studies by Kleinerman *et al* (1985) and Osterlind *et al* (1985), the majority did not receive radiation therapy.

In 1997, Neugut *et al* reported the results of a retrospective cohort study, using data from the Surveillance, Epidemiology, and End Results Programs (SEER) of the U.S. National Cancer Institute from 1973 – 1990 involving 141,761 patients with prostate carcinoma. In the cohort, 34,889 (24.6%) patients received radiation therapy (entire pelvis for the initial 45 – 50 Gy followed by a supplementary dose to the prostate only) and 106,872 (75.4%) received other treatments. Eight years after their radiotherapy for prostate carcinoma, the risk of bladder carcinoma increased among this sub-group of patients (RR = 1.5) but not for the majority of the patients who received other treatments. The risk of rectal carcinoma, acute nonlymphocytic leukemia (ANLL) and chronic lymphocytic leukemia was not elevated. The increased risk of bladder carcinoma was consistent with previous reports by Liskow *et al* (1987) and Greenberg *et al* (1988). The latency period between radiation therapy for prostate cancer and development of bladder carcinoma reported by Neugut *et al* (1997) was 5 or more years.

At the same time, Pawlish *et al* (1997) also conducted a retrospective cohort study using the same SEER data for the risk of SPCs among prostate cancer patients living in the Detroit Metropolitan area only involving 9,794 patients with microscopically confirmed, invasive prostate carcinoma during the period of January 1973 – December 1982. The standardized incidence ratio (SIR) was used to compare the number of SPCs observed in relation to the expected number. The total number SPC cases including all sites was 1,151 compared with an expected number of 1,144.74 thus making the SIR 1.01. The most common sites of SPC reported were lung and colon although only the urinary bladder was associated with a significantly increased risk of carcinoma (SIR = 1.57) among the patients. The risk of SPC in the lung was reduced (SIR = 0.83) compared with general population. Among 2,087 patients who received radiation as first-course treatment for prostate cancer and were followed up for at least 1 year, 272 (13%) developed one or more SPCs. In contrast, 628 (9.8%) of the 6,390 patients who did not receive radiation therapy developed SPC. It was concluded that there was a statistically significant difference in the age-adjusted SPC incidence rates between patients who did and did not receive radiation therapy as the first-course treatment. The incidence rate of SPC of all sites in the radiation sub-group was 1.43 times higher than that of the non-radiation sub-group.

In the study by Movsas *et al* (1998), the rate of SPCs in 543 prostate cancer patients, 3.9 years (mean) following radiation therapy at the Fox Chase Cancer Center (FCCC) was compared with the baseline data obtained from a study of 18,135 patients from the Connecticut Tumour Registry, 12.5% of whom received radiotherapy. It was observed that 1,053 (5.8%) of the patients from the

Connecticut Tumour Registry developed SPCs compared to 31 (5.7%) of the patients from FCCC. The radiation treatment technique used in FCCC was 4-field conformal radiotherapy with megavoltage X-rays (10 – 18 MV) at a rate of 2.1 Gy per day to a median dose of 72 Gy. It was concluded in this study that there was no increased risk of developing new neoplasm following prostate irradiation compared to rate expected from a larger population of patients with prostate cancer. Most (84%) of the second cancers observed at the FCCC occurred outside the radiation field and/or within 3 years of radiotherapy (97%). In addition, predisposing risk factors associated with lifestyles of the patients were suggested to be the cause of SPCs. However, providing that the radiation-induced SPCs are defined as tumours which develop ≥5 years after radiation from tissue within the irradiated field and have histopathologic features different from the primary tumours (Abdel-Wahab *et al* 2008), it is possible that a higher incidence number of SPCs would have been observed with longer follow-up periods. Furthermore, in this study majority (84%) of the second cancers were observed to occur outside the radiation field may be attributed to the dose outside the boundary of the primary collimator due to both leakage and scattered radiation especially when high-energy (≥10 MV) beams are used.

The study of Levi *et al* (1999) which involved 4,503 cases of prostate cancer collected from the cancer registries of the Swiss Cantons of Vaud and Neuchatel also came to conclusions similar to the earlier studies in that the incidence of SPCs was significantly reduced in men with prostate carcinoma. It was reported that a total of 380 SPCs were observed versus 534.1 expected SPCs (SIR = 0.7). However, as with previous studies, patient selection, under-registration of SPCs and lack of

surveillance among elderly patients contributed to the observed reduction in the risk of second malignancy. No information of treatment modes was provided in this study.

In the study of Chrouser *et al* (2005) involving a total of 1,743 prostate cancer patients who received external beam radiotherapy (EBRT) at the Mayo Clinic, Minnesota, the conclusion was that there was no increased risk of bladder cancer after radiotherapy among these patients in contrast to earlier studies by Neugut *et al* (1997) and Pawlish *et al* (1997). However, a short period of follow-up (mean of 7.1 years) after EBRT and under-reporting of SPCs are likely to contribute to the finding that SPCs of the bladder was not increased.

Brenner *et al* (2000) used the data from SEER (1973 – 1993) to compare the risk of second malignancies among patients with localized prostate carcinoma, 51,584 treated radiotherapy and 70,539 treated surgically without post-operative radiotherapy. Among the patients who had radiotherapy, 3,549 (6.9%) developed SPCs compared with 5,055 (7.2%) patients who had surgery without radiotherapy. Although the overall number of cases with second cancers showed that the observed incidence of SPCs was similar to the surgically treated patients, which are surrogates for that expected in the general population, when the data were analyzed for patients who were at ≤60 years of age at diagnosis, the SIR for all SPCs following radiotherapy increased to 1.05 compared with 0.89 for the whole patient group. The conclusion was that radiotherapy for prostate carcinoma was associated with a small but statistically significant increased risk of SPCs especially among the patients who survived the disease for 10 or more years. In relation to the specific sites of SPC, the relative risks of bladder, rectal and lung carcinoma

were increased following radiotherapy. It was concluded that the increased risks of SPCs among prostate cancer patients treated with radiotherapy was causally linked to the radiation exposure among younger (<60 years of age) long term survivors of the disease.

In the report of Brenner *et al* (2000) discussed above, the estimated absolute risk of radiation-induced second malignancy among prostate carcinoma patients was 1 in 290, increasing to 1 in 70 among long term (≥10 years) survivors. In 2002, Pickles and Phillips reported that the overall increased risk of SPCs among prostate cancer patients (British Columbia Tumour Registry, 1984 – 2000) undergoing radiotherapy was 1 in 220 with significant increased risks for colo-rectal cancers and sarcomas.

SEER data from 1973 to 1994 was used to evaluate the effect of radiation on the development of second primary rectal cancer among prostate cancer patients who survived the disease for at least 5 years after radiotherapy by Baxter *et al* (2005). An association between radiation treatment of prostate cancer and a moderate elevation in the risk of rectal cancer over time since the treatment was reported. The rate of rectal cancer after 10 or more years of follow-up among the 30,552 radiation-treated prostate cancer patients was 10 per 1,000 doubled compared with the 5.1 per 1,000 among the 55,263 patients treated with surgery.

In comparison to the study conducted by Movsas *et al* (1998) as discussed earlier, the findings reported by Baxter *et al* (2005) resulted from longer periods (mean of 9.0 years for radiation group) of follow-up. It has been discussed previously that potential radiation-induced SPC would take at least 5 years to develop. A significant increase in the risk of rectal cancer among long term survivors who

received radiotherapy for prostate cancer as reported by Baxter *et al* (2005) is an indication of the latency period in development of SPC and also a proof that there is a link between radiotherapy and risk of second malignancy.

Moon *et al* (2006) conducted a study involving 140,767 men with prostate cancer who remained alive 5 years after the date of their diagnosis to observe second cancer incidence after localized therapy for prostate cancer. In comparison to patients who received radiation therapy in form of radioactive implants or isotope either alone or in combination with EBRT, it was also observed that patients who received EBRT as only form of radiation treatments had statistically significant higher odds of SPCs in several organs either those which were located within or close proximity to prostate treatment volume like bladder (Odds Ratio [OR] = 1.63) and rectum (OR = 1.60) or at sites in the upper body and other areas not potentially related to radiation therapy such as colon (OR = 1.85), stomach (OR = 1.38), brain (OR = 1.83), and lung and bronchus (OR = 1.25). The odds ratio of second cancers of sigmoid colon, rectum, and bladder in patients who were treated with radioactive implants or isotope only were 0.25, 0.30, and 1.40 respectively. It was concluded in this study that despite the delivery of higher doses of radiation, patients who received radioactive implants had the lowest odds of developing a second cancer.

From these reports, the increased risks of SPCs in the bladder and rectum are suggested as likely to be associated with radiation treatment of the prostate cancer especially with EBRT techniques. Moon *et al* (2006) also suggested that the risks of SPC were also associated with brachytherapy. This is supported by Liauw *et al* (2006) who reported an increased risk of solid tumors of bladder, colo-rectum and

prostatic urethra 5 years after I-125 seed brachytherapy for prostate cancer. Most recently, Abdel-Wahab *et al* (2008) used SEER data (1973 – 2002) to determine the incidence of SPCs among various groups of patients with prostate adenocarcinoma. The overall incidence of SPC (regardless of age at diagnosis, race/ethnicity, and tumour grade) was higher among patients who received radiotherapy (8.8%) compared with the patients who did not undergo either radiotherapy or surgery (7.9%). Among the patients who received radiotherapy as primary treatment for prostate cancer, the highest incidence of SPC was found among those who received EBRT (10.3%) followed by the combination of EBRT and brachytherapy (5.7%) with the lowest incidence of SPC found among patients who received brachytherapy alone (4.7%). In addition, it was observed that most SPCs (81.7%) developed in organs located outside the pelvis with respiratory tumours being the most common non-pelvic second malignancies representing 21.9% for patients treated with radiotherapy. Analysis of data using multivariate Cox model revealed that relative risks (hazard ratio) of occurrence of late SPC (≥5 years after diagnosis of prostate cancer) in patients who received radiotherapy increase with times especially for brachytherapy, i.e. hazard ratio being 0.721, 0.930, and 1.200 at 5, 7, and 9 years respectively.

In summary, estimation of the risks of SPC from reported studies show highly heterogeneous results (Muller *et al* 2007). Comparisons between prostate cancer patients and the general population, regardless of treatment given suggested that the risks of SPC were reduced particularly in some earlier studies (Kleinerman *et al* 1985, Osterlind *et al* 1985, McCredie *et al* 1996, and Levi *et al* 1999). However, several more recent studies have reported increased risks of second malignancies

among prostate cancer patients treated with radiation therapy, particularly using external beam techniques alone (Brenner *et al* 2000, Pickles & Phillips 2002, Baxter *et al* 2005, Moon *et al* 2006, Liauw *et al* 2006, and Abdel-Wahab *et al* 2008).

Ron (1998) suggested that the cancer risks obtained from epidemiological studies could be used as the baseline in several issues such as setting the occupational and general population radiation exposure limits, decision making about the extent of cleanup necessary at nuclear sites, and determining the risk of radiation-induced cancer. However, there are factors which limit the utility of epidemiologic studies for cancer risk estimation including the risk of SPC after prostate cancer radiotherapy. Firstly, especially for the earlier studies discussed above, details of the radiotherapy delivery are limited or not available. Missing technical details of the treatment made it difficult to quantify the volume irradiated at risk (Liauw *et al* 2006). In addition, many studies do not include modern intensity-modulated radiotherapy or three-dimensional treatment techniques which deliver more localized radiation therapy, hence, introducing another source of possible bias (Abdel-Wahab *et al* 2008). Secondly, patient confounding factors such as age, race, lifestyle, and genetic predisposition always exist in the cohort of patients studied which adds to the difficulty of separating the influence of these factors from the radiotherapy in the estimation of risks of SPC following prostate irradiation.

In conclusion, with carefully conducted epidemiologic studies, while the risk of developing SPC may be associated with a variety of factors other than treatment, the link with radiation exposure has been established. A prospective study designed to minimize the influence of patient confounding variables is needed to accurately estimate the risk of second primary cancers to guide radiation

treatment decisions (Muller *et al* 2007) but would take too long to complete. A more simple and expeditious solution to these issues is proposed in the next section. The use of a radiobiological model designed to predict the risk of second primary cancer from radiodosimetric data of the organs at risk is demonstrated.

5.2.2 Estimation of second primary cancer risks using radiation dosimetric data and risk models

Apart from epidemiologic studies, measurements of radiation doses in normal organs/tissues located close to or at a distance to the planning target volume (PTV) can be used to estimate the risk of second primary cancer using existing models (Takam *et al* 2008). Radiation dosimetric data can be in the form of dose-volume histograms (DVHs) generated from the treatment plan of the particular radiation technique for organs/tissues located within or close to the PTV. Radiation dose data can also be obtained from direct measurement using various radiation dosimetry techniques. The appropriate risk estimation model is then applied to the dose data to determine the risk of second primary cancer.

The main sources of knowledge relating to the risks of radiation-induced cancer are derived from A-bomb survivors in Japan; from radiation accidents and from medically exposed individuals including exposure to radiation therapy (Hall & Wuu 2003). Although some data about induction of cancers has been collected from radiation accidents and medical exposures, the most recent Biological Effects of Ionizing Radiations (BEIR V) and The United Nations Scientific Committee on Effects of Atomic Radiation (UNSCEAR) reports base their risk estimates almost entirely on the data from survivors of the A-bomb attacks (Hall 2000).

The dose-response relationship for radiation-induced carcinogenesis for doses larger than 2 Gy is not clear, however, several estimates have been published. Schneider *et al* (2007) confidently expects that the relationship which best represents the real situation lies between the extremes of a linear and a linear-exponential model. In practice, using the data from A-bomb survivors which covers a range of doses from 0.005 to 4 Gy, the excess incidence for solid tumors was found to be a linear function of dose (Hall 2000). This model can be applied by multiplying the average absorbed dose with a risk coefficient to calculate the risk of radiation-induced carcinogenesis, assuming that the cells mutated by the radiation exposure survive the irradiation.

However, in clinical radiation therapy, the total dose delivered to patients is always larger than 2 Gy which could mean that the dose-response relationship for cancer induction is likely to be non-linear. In addition, the radiation dose is inhomogeneously distributed to organs at risk, parts of which will receive varying amounts of radiation dose. The concept of an average organ dose may not be applicable in this situation. Furthermore, when radiation doses larger than 2 Gy are delivered to the organs at risk, sterilization of the mutated cells within the organs becomes an important consideration since this counteracts the effect of mutation and subsequently of cancer induction.

The simplest approach to estimate the risk of SPC after radiotherapy is to first calculate the average organ/tissue dose and then to apply a linear risk coefficient corrected for dose and dose rate level. For example, assuming that a half of the organ receives a dose of 1 Gy and the other half is irradiated to 19 Gy, the average dose in the organ is simply 10 Gy (Schneider *et al* 2005). However, this method can

lead to errors in the risk estimation as it does not take into account the heterogeneity of the dose distribution in the irradiated organ/tissue (Dasu *et al* 2005). The estimated risk obtained using this method leads to an overestimate as the effect of cells sterilized by the dose of radiation is also not taken into account. Hence, this method is not applicable to clinical radiotherapy where the organs are usually exposed to radiation doses at both the low and high ends of the dose range.

Instead of using the simple average organ dose together with the linear risk coefficient to estimate the risk, the mean organ dose derived from the DVH in combination with a non-linear equation can be used which takes into account the competition between induction of mutations and cell survival (Dasu *et al* 2005). Although such model allows for the effect of sterilization of cells from exposure to high radiation doses, it does not fully account for the inhomogeneity of the radiation dose distribution over the entire irradiated organ and therefore is subject to errors in the calculation of the estimated risk. An example of an approach based on the concept of Organ Equivalent Dose (OED) to account for inhomogeneity of dose in organs at risk in the estimation of radiation-induced second malignancy following radiotherapy was proposed by Schneider *et al* (2005). Schneider *et al* used OED in the calculation of radiation-induced second primary cancer following 3D-CRT for Hodgkin's disease. Assuming that I_0^{org} is the low dose radiation-induced cancer incidence rate (absolute excess risk per 10,000 patients/year/Gy) of a fractionated radiotherapy schedule of a total dose D given in k fractions of dose d, the organ-specific cancer incidence rate after a single treatment session with a low dose is $I_0^{org} \times d$. The number of mutated stem cells which result in the development of the malignant growth is proportionally related

to the radiation-induced cancer incidence rate. However, following a single fraction of dose d, the total number of cells including the already mutated cells in the organ is, in a first approximation, reduced by $e^{-\alpha d}$ due to cells sterilization. Providing that I^{org} is the organ-specific cancer incidence rate (absolute excess risk per 10,000 patients/year) after prescription of the total dose D in k fractions, accordingly the cancer incident rate of an organ/tissue as a resulted fractionated irradiation is described by the following equation (Schneider *et al* 2005):

$$I^{org} = I_0^{org} De^{-\alpha_{org}D} ,\qquad\qquad (5.1)$$

where, I_0^{org} is the organ-specific cancer incidence rate for low dose irradiation as defined earlier and α_{org} is an organ-specific cell sterilization parameter.

A dose-response curve for radiation-induced cancer of a specified organ can be derived from equation (5.1). The OED for radiation-induced cancer of the irradiated organ is then obtained from the equation as follows (Schneider *et al* 2005):

$$OED_{org} = \frac{1}{N}\sum_{i=1}^{N} D_i e^{-\alpha_{org}D_i} ,\qquad\qquad (5.2)$$

where the sum is taken over N dose calculation points in the same constant volume of the organ. OED is the dose (in Gy) distributed uniformly over the entire organ/tissue which causes the same radiation-induced cancer incidence as that if it was inhomogeneously distributed within the same organ. The risk of radiation-induced second primary cancer is estimated from the dose-response curve thus derived from equation (5.1).

In the risk estimation model described above, I_0^{org} and α_{org} are parameters which need to be known. The organ-specific cancer incidence rate at low radiation dose (I_0^{org}) can be obtained from the atomic bomb survivor data whilst the organ-specific cell sterilization parameter (α_{org}) needs to be estimated from experiments. It has been suggested that the precision of the OED concept in the estimation of SPC risk is mainly dependent on the precision of the determination of α_{org} for the different organs (Schneider *et al* 2005).

To fully take into consideration of the inhomogeneity of the dose distribution across the entire volume of an irradiated organ as a result of radiotherapy, a non-linear competition model should be used to estimate risk at each dose interval of the DVH. Integration of these risks across the actual dose distribution over the entire organ volume would then yield the final result (Dasu *et al* 2005). This is the basis of the competitive risk model used in estimation of the risk of radiation-induced SPC developed by Dasu *et al* (2005) from the concept proposed by Gray (1965)(see Hall 2006). In this thesis, this model is used to estimate the risk of second primary cancer in several organs-at-risk following various techniques of radiation therapy for prostate cancer.

In the UNSCEAR model of radiation-induced carcinogenesis, the general equation of which is based on the linear quadratic (LQ) model of radiation effects, the total radiation effect in terms of risk is the product between the probabilities of inducing DNA mutations and survival of the irradiated cells. This radiation effect is defined by Dasu *et al* (2005) and Gray (1965) as:

$$Effect = \left(\alpha_1 D + \beta_1 D^2 \right) \times e^{-\left(\alpha_2 D + \beta_2 D^2 \right)}, \tag{5.3}$$

where D is the dose delivered in a single exposure, α_1 and β_1 are the linear and quadratic coefficients for induction of DNA mutations, and α_2 and β_2 are the linear and quadratic coefficients for cell kill (UNSCEAR 1993).

The first term of equation (5.3) represents the induction of DNA mutations whilst the second term represents the cell survival. The equation, therefore, describes risk of mutation of the irradiated surviving cells after a single radiation dose, D. It is notable that for very low doses, the quadratic component of the second term in equation (5.3) approaches unity and becomes negligible thus making the dose-effect relationship approximately linear with α_1, the slope of the curve. For this situation, the first term of the equation can be assumed to be equal to the risk coefficients derived from epidemiological population studies of low dose irradiation (Dasu *et al* 2005).

In clinical radiotherapy, the organs-at-risk are usually exposed to a range of fractionated radiation doses as described earlier. Therefore, equation (5.3) needs to be modified to reflect this. Assuming firstly that the radiation dose fraction affects DNA mutation and cell killing of the organ/tissue equally, the effect on the risk of radiation-induced SPC can be expressed (Dasu *et al* 2005) as:

$$Effect = \left(\alpha_1 D + \frac{\beta_1 D^2}{n} \right) \times exp\left[-\left(\alpha_2 D + \frac{\beta_2 D^2}{n} \right) \right], \qquad (5.4)$$

where D is the total dose given in n fractions. As discussed for equation (5.3) earlier, for very low doses the quadratic component of the second term in equation (5.4) becomes negligible and the risk approximates to a linear function of dose with α_1 the slope of the dose-effect curve.

The equation (5.4) is then applied for each dose interval in the DVH of the organ-at-risk and the total effect is obtained by integrating the effects on the dose intervals using the following equation (Dasu *et al* 2005):

$$Total\ effect = \frac{\sum_i \left(v_i \times Effect(D_i) \right)}{\sum_i v_i}, \qquad (5.5)$$

where v_i is the volume of organ/tissue receiving dose D_i delivered in n individual fractions and $Effect(D_i)$ is the non-linear dose-response relationship of the competition model.

As discussed earlier, the main advantage of the competitive risk model is that it allows the DVH of the irradiated organ/tissue to be used without the need to transform all the dose intervals into a single uniform dose value which does not accurately reflect the actual clinical situation. Therefore, the model accounts for the effects of dose-distribution inhomogeneity in the risk estimation of SPC. It also allows for the two competitive processes of DNA mutation and cell kill as a result of the wide range of radiation doses the organ at risk is exposed to in clinical radiotherapy to be incorporated in the risk estimation.

The competitive risk model is based on the hypothesis that the probability of second primary cancer increases with increasing radiation dose initially until a peak is reached and then decreases due to the predominance of cell kill effects (Harrison 2004). This reflects the skewed bell-shape dose-effect curve of the competitive risk model shown in Figure 5.1 below.

NOTE:
This figure is included on page 151
of the print copy of the thesis held in
the University of Adelaide Library.

Figure 5.1. *The plots show the predicted second primary cancer risks of rectum, bladder, and urethra following prostate cancer standard (2 Gy) fractionated 3D-CRT using the competitive risk model. The bell-shape dose-effect curve exhibits the result of two competing processes, with increasing dose induction of DNA mutation dominating at low doses and the predominance of cell kill at higher doses. Parameters used in calculation are listed in Table 5.1 and were taken from Dasu et al (2005).*

The report of Dorr and Herrmann (2002) provides support for the clinical applicability of the competitive risk model. They reported that the majority (58%) of SPCs occurred within the margin around the treatment volume where organs-at-risk received radiation doses of ≤ 6 Gy. The study involved 85 patients treated with radiotherapy for their primary tumours that met selection criteria for spatial relation between new tumour and primary treatment field. Approximately 35% of the SPCs developed at doses between 10 and 30 Gy and only 7% were found within the volume of tissue of organ-at-risk receiving radiation doses larger than 30 Gy. The results of this study are consistent with the dose-response relationship in terms of radiation-induced carcinogenesis predicted by the competitive risk

model. However, it has been previously reported that some SPCs occur in areas which received radiation doses as large as 65 Gy (Dorr & Herrmann 2002). Hall and Wuu (2003) have also reported that there was no significant change in the relative risk of bladder carcinogenesis when radiation doses of between 2 and 80 Gy are delivered to the organ-at-risk in the radiation treatment of cervical and prostate carcinoma. These reports are however consistent with the existence of a plateau in the probability of radiation-induced carcinogenesis at higher radiation doses. There has been no data over the wide range of fractionated doses the organs-at-risk are exposed to in clinical radiotherapy to support the contention of a plateau in risk of induction of SPC at higher radiation doses. The International Committee on Radiation Protection (ICRP) based implicitly on a linear dose response in relation to cancer induction probabilities is currently the most appropriate guide to permissible radiation dose limits for occupational exposure (Harrison 2004). However, the competitive risk model of SPC risk estimation for organs-a-risk used in this thesis may provide more appropriate basis to compare the SPC risks corresponding to various radiotherapy techniques used in the treatment of prostate cancer.

5.3 Methods – risk estimation

The risk of second primary cancers of rectum, bladder, and urethra after various radiation therapy techniques which have evolved in the Department of Radiation Oncology, RAH, for the treatment of localized prostate cancer is estimated using the competitive risk model (Dasu *et al* 2005). These treatment techniques include standard fractionated (2 Gy) 4-field 3D-CRT (to 64 Gy total dose), hypofractionated (2.75 Gy) 4-field 3D-CRT (to 55 Gy total dose), standard fractionated 4-field 3D-

CRT (to 70 Gy and 74 Gy total dose), standard fractionated 5-field 3D-CRT (to 70 Gy total dose), HDR-BT alone (monotherapy) and HDR-BT combined with standard 4-field 3D-CRT (combined-modality treatment), and LDR-BT monotherapy. Details of the various radiation treatment techniques and the derivation of the dose-volume histograms (DVHs) of the organs-at-risk retrieved from the corresponding radiation treatment plans are provided in Chapter 4 sections 4.1 and 4.2 of this thesis. In summary, 211 DVHs of the organs-at-risk from the real treatment plans of 101 patients treated with the various radiation treatment techniques were first retrieved from the corresponding planning systems. The DVHs based of non-standard fractionated radiation doses were then converted to Biological Effective Dose-Volume Histograms ($BE_{ff}DVHs$) and then to Equivalent Dose-Volume Histograms ($D_{eq}VHs$) as detailed in Chapter 3. Finally, the risk of second primary cancers of the organs-at-risk were calculated by applying equations (5.4) and (5.5) of the competitive risk model to the $D_{eq}VHs$. While acknowledging that using different groups of patients to compare the various radiotherapy techniques introduces another variable into the study, this approach allows the risk estimates to be correlated with real patient data.

The model parameters for the organs-at-risk in question of   ,   ,   ,and   are derived from the report by Dasu *et al* (2005) and summarized in Table 5.1.

Table 5.1. The competitive risk model parameters used for estimation of the SPC risk following various radiation treatment techniques for prostate (Dasu et al 2005).

NOTE:
This table is included on page 153 of the print copy of the thesis held in the University of Adelaide Library.

5.3.1 Differential DVHs of organs-at-risk

Figures 5.2 and 5.3 show differential DVHs of rectum retrieved from treatment plans for 4-field 3D-CRT to total dose 70 Gy or 74 Gy and 5-field 3D-CRT respectively. Two distinctive patterns of dose distribution can be seen from these examples. In Figure 5.2 differential DVH P1 and P4 show that the rectum was exposed to equivalent doses mostly in the high-dose region whereas P2 indicates that the rectum was exposed to a wide-range of equivalent doses. These patterns of dose distribution are typical of 4-field EBRT techniques (see Figures 4.1, 4.2, and 4.6). Exposure of rectum to equivalent doses in the low-dose region was observed more frequently with 5-field CRT (Figure 5.3) as the treatment beams do not directly traverse the rectum as with the 4-field CRT technique.

In this and following sections, mean equivalent dose ($\overline{D_{eq}}$) and S.D of a particular organ in any patient treated with a specific treatment technique are calculated from a DVH using the following equations:

$$\overline{D_{eq}} = \frac{\left(D_{eq} \times v_{diff}\right)}{V},$$ (5.6)

and $$S.D = \left[\sum\left(\frac{v_{diff} * \left(D_{eq} - \overline{D_{eq}}\right)^2}{V}\right)\right]^{\frac{1}{2}},$$ (5.7)

where v_{diff} is the differential volume in the DVH which received dose equivalent D_{eq} and V is the total irradiated volume of the organ in consideration.
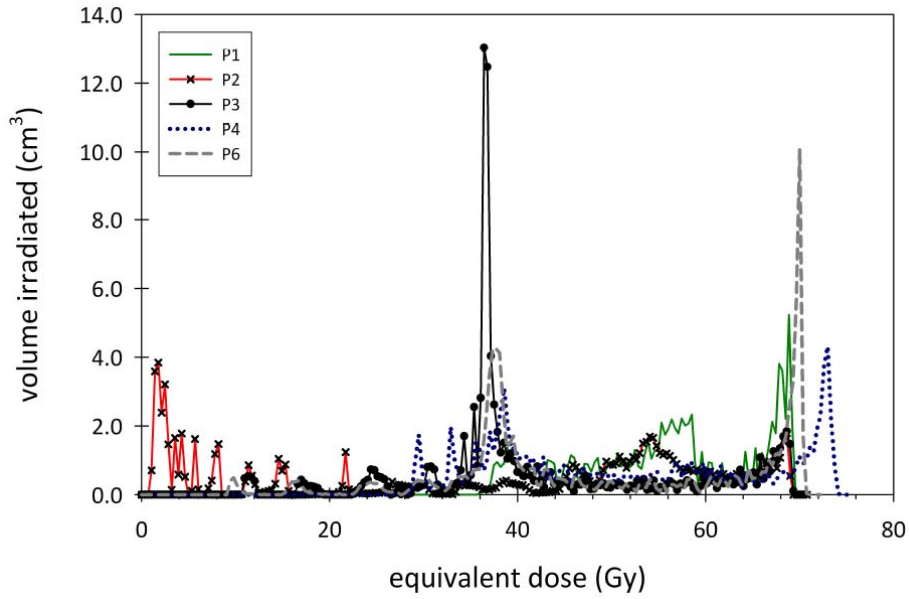
Figure 5.2. Differential DVH of rectum taken from radiation treatment plans for 4-field 3D-CRT to total dose 70 Gy or 74 Gy. Differential DVH P2 is an example of a plan which results in irradiation of rectum to equivalent doses (3 – 6 Gy) where DNA mutations dominate resulting in higher risk of SPC compared with P4 and P6 (see results in section 5.4).
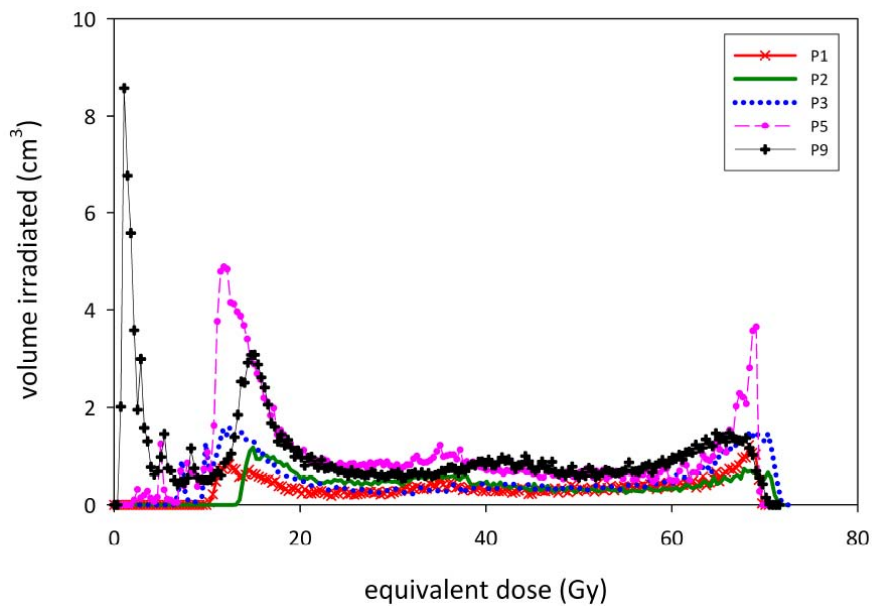

Figure 5.3. Differential DVH of rectum taken from radiation treatment plans for 5-field 3D-CRT technique. Similar to 4-field 3D-CRT/70 or 74 Gy radiation treatment plans, rectal differential DVHs in 5-field 3D-CRT plans which result in irradiation of rectum to equivalent doses around 3 – 6 Gy (DVH P3, P5 and P9) are associated with higher risks of SPC compared with P1 and P2 where equivalent doses are uniformly spread across the range (see results in section 5.4).

155

For HDR-BT and LDR-BT as monotherapy (see Figure 4.7 and 4.8), comparatively small volumes of rectum were irradiated to high equivalent doses, the average of mean equivalent doses ± S.D being 59.8 ± 8.3 Gy and 61.9 ± 5.8 Gy, respectively. It is also evident from Figures 4.7 and 4.8 that most of the rectum was exposed to negligibly low equivalent doses when using brachytherapy techniques.

Differential DVHs of the bladder from the plans of standard and hypofractionated 4-field 3D-CRT, 4-field 3D-CRT/70 or 74 Gy as well as 5-field 3D-CRT plans are similar to the differential DVHs of the rectum. For example, in the plans of 4-field 3D-CRT/70 Gy (Figure 5.4) some DVHs (e.g. P7) of the bladder received predominantly high equivalent doses in contrast to others (e.g. P2) where the bladder was exposed largely to low equivalent doses while in yet others (e.g. P1 and P9) the bladders was exposed to a wide-range of equivalent doses.
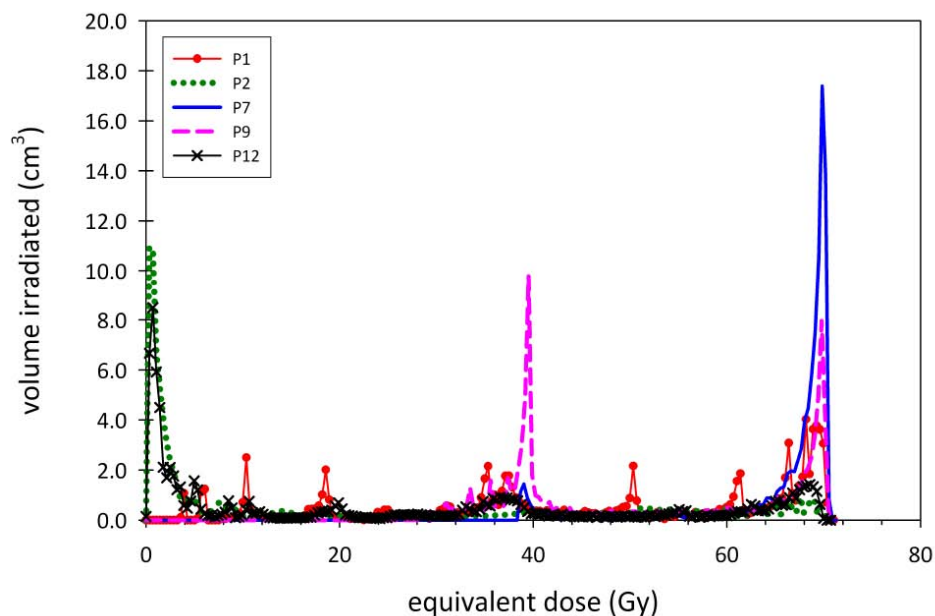

Figure 5.4. Differential DVHs of bladder taken from radiation treatment plans for 4-field 3D-CRT/70 Gy. In P2 and P12 the bladder received some equivalent doses resulting in higher risks of SPC compared to high equivalent doses in P1, P7, and P9 which were associated with lower risks of SPC (see results in section 5.4).

The differential DVHs of urethra (see Figure 4.14 and 4.15) indicated that the volume of this critical structure was mostly irradiated to very high equivalent doses especially from LDR-BT and HDR-BT techniques. The average of mean equivalent doses which irradiated to urethra as the results of standard fractionated 3D-CRT, hypofractionated 3D-CRT, HDR-BT, and LDR-BT were 64.2 ± 0.6 Gy, 59.3 ± 0.1 Gy, 93.5 ± 5.7 Gy, and 130.4 ± 5.1 Gy, respectively.

5.4 Results – estimated risks of SPC in organs-at-risk

5.4.1 Rectum

The risk of developing SPC of rectum associated with each of the various radiation treatment techniques is shown in Table 5.2. For the treatments involving EBRT, average predicted risk of rectal carcinogenesis associated with 5-field 3D-CRT to total dose of 70 Gy was the highest (0.2 ± 0.1%) followed by 4-field 3D-CRT to total dose of 70 Gy (0.08 ± 0.2%), combined-modality treatment (0.06 ± 0.1%), hypofractionated 3D-CRT (0.02 ± 0.02%), standard fractionated 3D-CRT (0.01 ± 0.01%), and 4-field 3D-CRT to total dose of 74 Gy (approximately 0.002%). In contrast, the estimated risk of rectal SPC associated with the HDR-BT and LDR-BT as monotherapy techniques was only ~0.0001% and 0.0002% respectively. This is associated with the equivalent dose conversion of the physical dose-based differential DVHs of this organ-at-risk which resulted in shifting of the physical doses given to volumes of rectum to higher equivalent doses where the associated risk of SPC is very small. $BE_{ff}DVHs$ of rectum for HDR-BT (Figure 4.7) and LDR-BT (Figure 4.8) as monotherapy techniques were shown in Chapter 4.

Table 5.2. *Average estimated risk of rectal SPC associated with various prostate cancer treatment techniques applying the competitive risk model to dosimetric parameters.*

Treatment Technique	No. of DVH/ patient	Average of Mean Equivalent Dose in Gy ± S.D (range)	Average Irradiated Volume in cm³ ± S.D (range)	Average Second Primary Cancer Risk in % ± S.D (range)
Standard fractionated 3D-CRT (64 Gy at 2 Gy/fraction)	7	48.5 ± 4.1 (41.6 – 53.6)	93.9 ± 44.4 (54.6 – 186.6)	0.01 ± 0.01 (0.00 – 0.04)
Hypofractionated 3D-CRT (55 Gy at 2.75 Gy/fraction)	10	43.9 ± 2.0 (39.6 – 46.2)	83.8 ± 28.0 (45.9 – 142.5)	0.02 ± 0.02 (0.00 – 0.06)
4-field 3D-CRT				
A. To total dose of 70 Gy	13	46.5 ± 5.5 (38.1 – 55.8)	72.0 ± 31.1 (25.3 – 141.7)	0.08 ± 0.16 (0.00 – 0.6)
B. To total dose of 74 Gy	3	51.6 ± 0.6 (50.8 – 52.0)	62.7 ± 9.8 (51.8 – 70.9)	1.9×10^{-3} $\pm 1 \times 10^{-3}$ (1.1×10^{-3} – 2.7×10^{-3})
5-field 3D-CRT (70 Gy at 2 Gy/fraction)	14	38.6 ± 5.7 (30.2 – 51.6)	98.5 ± 51.9 (36.6 – 204.5)	0.2 ± 0.1 (0.01 – 0.5)
Combined-modality Treatment (3D-CRT & HDR-BT)	8	69.4 ± 6.1 (60.4 – 79.2)	90.1 ± 54.6 (42.7 – 215.5)	0.06 ± 0.1 (0.01 – 0.4)
HDR-BT (Ir-192) monotherapy (4 * 9.5 Gy)	9	59.8 ± 8.3 (49.6 – 78.5)	5.4 ± 2.6 (2.1 – 8.1)	1.0×10^{-4} $\pm 1 \times 10^{-4}$ (5.9×10^{-7} – 3.2×10^{-4})
LDR-BT (I-125) monotherapy	37	61.9 ± 5.8 (50.5 – 73.3)	3.4 ± 1.0 (1.5 – 5.3)	2.0×10^{-4} $\pm 3 \times 10^{-4}$ (8.4×10^{-6} – 1.2×10^{-3})

When inspecting the converted equivalent dose volume histograms, there is no volume of rectum receiving equivalent doses in the range where the risk of SPC is high (3 – 5 Gy). This is clearly a result of conversion of the physical doses (9.5 Gy/fraction) to equivalent doses (2 Gy/fraction) which shifted the doses towards higher values, for example, 1.5 Gy of physical dose (at 9.5 Gy/fraction) was converted to 36 Gy of equivalent dose (at 2 Gy/fraction).

5.4.2 Bladder

The risks of developing bladder cancer associated with the brachytherapy (both HDR and LDR) techniques could not be estimated because the full extent of the bladder could not be contoured from the ultrasound based planning system. Among the external beam irradiation techniques, the risk of bladder second primary cancer in 5-field 3D-CRT to total dose of 70 Gy was the highest being 0.1 ± 0.1% (Table 5.3). The risk of bladder carcinogenesis in association with 4-field 3D-CRT to total dose of 70 Gy and 74 Gy averaged 0.08 ± 0.11% and 0.05 ± 0.06%, respectively. The average risk of bladder cancer for standard and hypofractionated 3D-CRT was approximately 0.002% and 0.001%, respectively. It can be noticed that the risks of SPC for standard and hypofractionated 3D-CRT are smaller than the risks of SPC in rectum for the same treatment technique.

Table 5.3. Average estimated risk of bladder carcinogenesis associated with various prostate cancer treatment techniques applying the competitive risk model to dosimetric parameters.

Treatment Technique	No. of DVH/ patient	Average of Mean Equivalent Dose in Gy ± S.D (range)	Average Irradiated Volume in cm³ ± S.D (range)	Average Second Primary Cancer Risk in % ± S.D (range)
Standard fractionated 3D-CRT (64 Gy at 2 Gy/fraction)	7	53.4 ± 4.1 $(44.6 - 56.4)$	133.4 ± 32.9 $(90.7 - 181.0)$	$2.2 \times 10^{-3} \pm 3 \times 10^{-3}$ $(1.8 \times 10^{-4} - 8.2 \times 10^{-3})$
Hypofractionated 3D-CRT (55 Gy at 2.75 Gy/fraction)	10	50.8 ± 4.3 $(42.8 - 54.9)$	119.6 ± 42.3 $(56.0 - 184.6)$	$1.3 \times 10^{-3} \pm 2 \times 10^{-3}$ $(7.4 \times 10^{-5} - 4.2 \times 10^{-3})$
5-field 3D-CRT (70 Gy at 2 Gy/fraction)	14	43.0 ± 12.2 $(20.4 - 63.7)$	162.4 ± 99.2 $(46.6 - 456.8)$	0.1 ± 0.1 $(0.0 - 0.3)$
4-field 3D-CRT				
A. To total dose of 70 Gy	13	48.3 ± 13.3 $(20.6 - 65.5)$	161.7 ± 72.6 $(81.5 - 306.0)$	0.08 ± 0.11 $(0.0 - 0.3)$
B. To total dose of 74 Gy	3	44.2 ± 6.3 $(37.9 - 50.5)$	199.4 ± 147.9 $(72.4 - 361.8)$	0.05 ± 0.06 $(0.0 - 0.1)$

5.4.3 Urethra

In calculating the average risk of second primary cancer, the prostatic urethra was assumed to receive the same homogeneous equivalent doses as prescribed to the prostate for each EBRT technique. For the HDR and LDR brachytherapy techniques small fractions of the urethra received even higher equivalent doses (up to 200 Gy) than the dose prescribed to the prostate. The exposure to such high radiation doses resulted in very small risks of developing second primary cancer for urethra as predicted by the CR model. The risk of urethral second primary cancer

associated with the various prostate treatment techniques are summarized in Table 5.4.

Table 5.4. *Average estimated risk of urethra SPC associated with various prostate cancer treatment techniques applying the competitive risk model to dosimetric parameters.*

Treatment Technique	No. of DVH/ patient	Average of Mean Equivalent Dose in Gy ± S.D (range)	Average Irradiated Volume in cm^3 ± S.D (range)	Average Second Primary Cancer Risk in % ± S.D (range)
Standard fractionated 3D-CRT (64 Gy at 2 Gy/fraction)	7	64.2 ± 0.6 (63.8 – 65.3)	5.2 ± 0.5 (4.6 – 5.9)	$1.2 \times 10^{-10} \pm 3 \times 10^{-11}$ ($6.7 \times 10^{-11} – 1.5 \times 10^{-10}$)
Hypofractionated 3D-CRT (55 Gy at 2.75 Gy/fraction)	10	59.3 ± 0.1 (59.2 – 59.4)	5.5 ± 1.1 (4.3 – 7.5)	$4.1 \times 10^{-11} \pm 1 \times 10^{-11}$ ($3.0 \times 10^{-11} – 5.5 \times 10^{-11}$)
HDR-BT (Ir-192) monotherapy (4 * 9.5 Gy)	10	93.5 ± 5.7 (83.7 – 103.4)	0.8 ± 0.3 (0.5 – 1.5)	$2.5 \times 10^{-6} \pm 7 \times 10^{-6}$ ($3.9 \times 10^{-13} – 2.1 \times 10^{-5}$)
LDR-BT (I-125) monotherapy	36	130.4 ± 5.1 (118.0 – 139.2)	0.6 ± 0.2 (0.2 – 1.6)	$2.6 \times 10^{-9} \pm 1 \times 10^{-8}$ ($1.4 \times 10^{-15} – 8.6 \times 10^{-8}$)

5.5 Discussion

Discussions on distributions of equivalent doses in the volumes of organs-at-risk including rectum, bladder, and urethra have been presented in Chapter 4. Differential DVHs of the organs-at-risk used in estimations of SPC risks are the same which were used for NTCP estimations. Therefore, discussion on the impact of differential DVHs uncertainties on risk of SPC induction will not be repeated in this chapter.

The risks of SPC associated with a particular radiation treatment technique for prostate cancer have been reported (Moon *et al* 2006, Liauw *et al* 2006, Hall & Wuu 2003, and Hall 2006). Brenner (2006) suggested that by combining the incidence of all second cancers, the risk of SPCs in long-term survivors of prostate cancer increases among those treated by radiotherapy compared to those who had surgery. The work in this thesis represents the first attempt to estimate and compare the risks of developing SPC of organs-at-risk of all current widely available radiation treatment techniques for prostate cancer by applying the competitive risk model to the differential DVHs. Although the average risks of development of SPC are shown to be small ($\leq$0.6%), notable differences nonetheless exists among the radiation treatment techniques, being generally higher for the described EBRT techniques compared with brachytherapy (both LDR and HDR) as monotherapy techniques.

The competitive risk model of SPC induction includes the two competing events: (a) DNA mutations of cells in the radiation field and (b) cells killed as a result of the radiation exposure, particularly cells of the organs-at-risk. Most of the plans, derived from the various radiation treatment techniques in this study, resulted in irradiation of organs-at-risk to equivalent doses in the range where cell killing is dominant thus accounting for the small ($\leq$ 0.6%) overall predicted risks of developing SPC.

The estimated risk of developing a radiation-induced SPC has been estimated as 1 in 290 in absolute terms for all prostate carcinoma patients treated with radiotherapy, increasing to 1 in 70 for long term ($\geq$ 10 years) survivors (Brenner *et al* 2000). This estimate is supported by a clinical study which reported that the

overall increased SPC risk for prostate cancer patients treated with radiation therapy was 1 in 220 (Pickles *et al* 2002). The calculated risks of SPC of organs-at-risk in this current work are consistent with previous reports although radiobiological parameters based on non-uniform distribution of doses over the organs-at-risk and the effect of different fractionation schedules have been included in the risk calculations. The model used in thesis does not, however, account for confounding factors such as age, smoking and dietary habits of patients which have been reported to influence the incidence of SPC in organs-at-risk following radiation therapy for prostate cancer (Rheingold *et al* 2003). In addition, the competitive risk model cannot predict time of induction and manifestation of the SPC after radiation exposure even though it has been suggested that the relative risk of SPCs for prostate patients treated by radiotherapy increases with time after exposure to treatment (Liauw *et al* 2006 and Abdel-Wahab *et al* 2008).

HDR and LDR brachytherapy as monotherapy were associated with the lowest risk of development of SPC which is attributable to the delivery of high equivalent doses to small volumes of normal tissues inherent in the techniques. In contrast, higher predicted risks were obtained in the treatment plans involving EBRT techniques such as standard fractionated and hypofractionated 3D-CRT. 5-field 3D-CRT technique (to total dose of 70 Gy) in particular has higher calculated risk of SPC as the beams do not pass through rectum directly, leaving rectum exposed to lower doses of radiation at which DNA mutations in organs-at-risk dominate.

The use of EBRT alone for treatment of prostate cancer, as shown in this study, resulted in irradiation of larger volumes of organs-at-risk to lower dose equivalents which accordingly led to higher risks of SPC induction compared to

HDR-BT or LDR-BT as monotherapy techniques. It was also observed in this study that the use of HDR-BT as a boost to EBRT in combined-treatment modality technique could reduce the risk of SPC associated with EBRT monotherapy particularly when higher total doses (70 Gy or 74 Gy) are prescribed. In addition, hypofractionated 3D-CRT technique was also associated with lower risks of SPC of bladder and urethra compared to standard fractionated 3D-CRT except for rectum. A lower prescription dose (55 Gy at 2.75 Gy per fraction) could be the cause of these reduced risks due to less exposure of surrounding healthy organs to leakage and scattered radiations. However, this effect was not observed in rectum where its risk of SPC associated with hypofractionated 3D-CRT was comparable to that of standard fractionated 3D-CRT.

The data from this study has important implications for the radiation treatment of prostate cancer and suggests that either form of brachytherapy is optimal for the low risk prostate cancer, particularly for younger (≤70 years old) patients who are likely to survive long enough for the predicted risks to increase further. Our data highlights the need to be circumspect about the use of multiple (≥5) photon field techniques to achieve better dose distribution and conformality in external beam radiotherapy and suggest a role for inclusion of risk of SPC in treatment planning systems to assist in the choice of a suitable treatment plan.

In this study the model assumes that the development of SPC is a result of the competitive mechanisms between induction of genetic transformation of cells in organs-at-risk and death of these cells. Risk of developing SPC in irradiated normal tissues rises as radiation dose increases to a maximum at doses around 3 – 5 Gy. With further increases in radiation dose, the cell kill effect becomes dominant and

causes a reduction in survival of transformed cells. Consequently, the risk of developing SPC reduces as well. The dose-response relationships in terms of risk of SPC applied in competitive risk model seem to fit well in the third scenario described by Ruben *et al* (2008) which is that the risk decreases with increasing dose because of the cell kill effect at high doses. However, the existence of phenomena like bystander effect (increase in cell kill in a sub-population), adaptive response (cells previously sensitized by radiation exposure have diminishing response to increasing radiation doses, i.e. increased cell survival), and uncertainty of dose-response at high doses may alter the final results of risk calculation using competitive risk model. At the time of this study, additional radiobiological parameters addressing the effects of such phenomena for integration into the existing model are not yet available. However, it is reasonable to assume that predicted risks of SPC obtained with competitive risk model in this study, which takes into account effects at low and high normal tissue exposures in radiation therapy, have been reasonably estimated in the current circumstances using the information available.

5.6. Conclusion

Among all the radiation treatment techniques for prostate cancer evaluated for the risks of SPC induction in organs-at-risk, either LDR or HDR brachytherapy offer smaller risks of carcinogenesis compared to treatments involving EBRT techniques. For the techniques involving EBRT, those which include more treatment fields result in exposure of larger volumes of organs-at-risk to lower radiation doses but higher risks of SPC. The data has important clinical

implications for choice of radiation modality and plans for the treatment of prostate cancer.

Based on the result showed in chapters 4 and 5, the clinician might need to weigh the risks of NTCP and SPC when choosing a particular treatment modality for prostate cancer. While in general, it is the early and late treatment complications that are considered to be the most important factors affecting a decision, for a particular group of patients of young age and long expected survival, the SPC estimate should be considered as well.

Chapter 6

Enriched lithium-6 and lithium-7 LiF:Mg,Cu,P glass-rod thermoluminescence dosimeters and out-of-field radiations dosimetry

6.1 Introduction

Previously in chapters 4 and 5, the Normal Tissue Complications Probability (NTCP) and the risk of radiation-induced Second Primary Cancers (SPCs) in organs-at-risk after prostate cancer radiotherapy were presented. In those chapters only organs lying in the high dose gradient, i.e. in the proximity to the target volume, were considered. These organs are generally irradiated to high radiation doses leading to high probability of normal tissue complications and usually to a small risk of radiation-induced SPCs. However, with the current

practice of prostate cancer external beam radiation therapy where high-energy (up to 25 MV) medical linear accelerators are used routinely to produce photon beams, there are leakage and scattered out-of-field radiations produced from the primary radiation beams. In addition, it is well known that high-energy photons (above 8 MeV) also produce neutrons by interacting with the constituents of accelerator structures and the treatment room as well as with the patient (d'Errico *et al* 1998). Neutron fluence spectra produced from interactions between bremsstrahlung X-rays and high Z materials such as tungsten target and other components in the head of a medical linear accelerator are shown in Figure 6.1 (Huang *et al* 2005). The average neutron energy ranges from 0.401 MeV – 0.798 MeV depending on the incident electron beam energy.
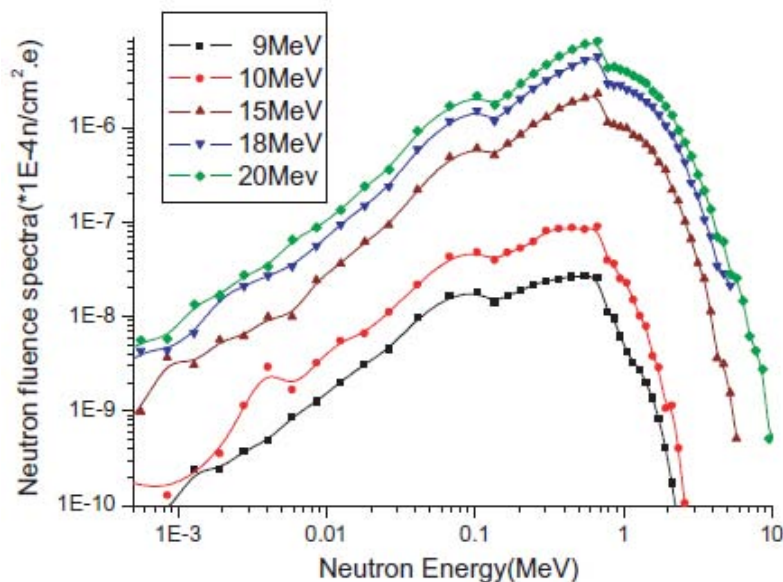

Figure 6.1. *Neutron fluence spectra produced from interactions between different incident electron beam energies and tungsten target in the head of electron linear accelerators (Huang et al 2005). The spectra were calculated using FLUKA Monte Carlo simulation code.*

These out-of-field radiations irradiate organs located within or around the prostate targeted area as well as organs located distally from the treatment volume. In order to evaluate the effects of radiation exposure in such organs especially in terms of radiation-induced second primary cancers, there is a need to develop a technique which can determine radiation doses at various locations around the linear accelerator and inside the humanoid phantom. In this chapter, radiation dosimetry technique is proposed for measurement of the out-of-field photon and neutron doses resulting from irradiation by a high-energy (18 MV) Varian iX medical linear accelerator (Varian Medical System, CA).

In general, the out-of-field dose from photons was observed to be strongly dependent on the distance from the field edge (Howell *et al* 2006) and the photon dose rate was the highest around the isocentre (Vanhavere *et al* 2004). However, the neutron dose rate appeared to be more constant with distance from the isocentre (Figure 6.2).
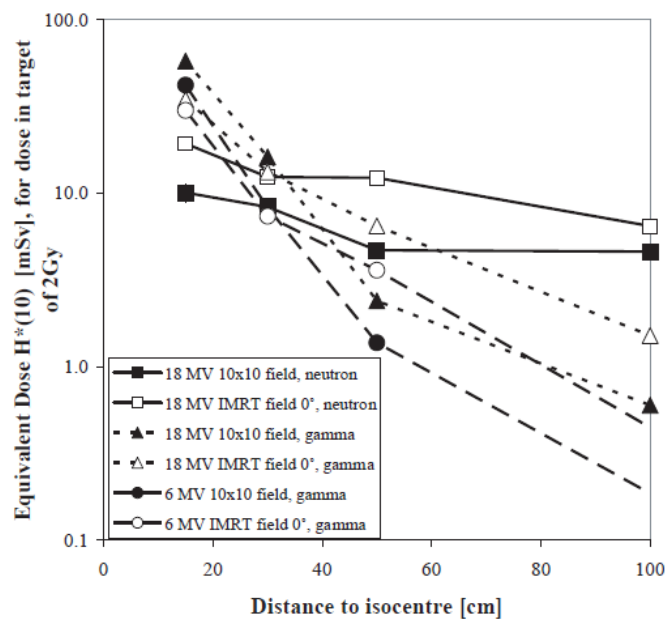

Figure 6.2. *Free-in-air photon and neutron doses for 6 MV and 18 MV IMRT prostate radiotherapy techniques with different field-sizes and angles (Vanhavere et al 2004).*

Hence, at some point along the patient plane, the neutron doses are comparable or larger than the photon doses resulting in a larger neutron to photon absorbed dose ratio (Carinou *et al* 2005). The average energy of neutrons produced from 18 MV medical linacs was found to range between 0.5 – 1.2 MeV (Lin *et al* 2001 [Siemens Primus], Huang *et al* 2005 [FLUKA Monte Carlo simulation], Facure *et al* 2005 [MCNP Monte Carlo simulation], Howell *et al* 2006 [Varian Trilogy & 23EX]). However, for 18 MV beam, the most probable neutron energy produced is 0.5 MeV (Facure *et al* 2005). Howell *et al* (2006) have also found that the linac with beam energies of 18 MV resulted in higher effective dose to normal organs compared with 6 MV largely due to neutron contribution.

Measuring neutrons is important as they have higher radiation weighting factor (W_R) than photons ($W_R = 1$) resulting in higher Relative Biological Effectiveness (RBE). According to the Report No. 92 of the International Commission on Radiation Protection (ICRP), the neutron W_R is defined as a continuous function of the incident neutron energy and can be written as:

$$W_R = 5 + 17 exp\left(-\left(ln\left(2E_n\right)\right)^2 / 6\right), \qquad (6.1)$$

where E_n is the neutron energy in MeV.

Table 6.1 shows neutron W_R values as a function of incident neutron energy (E_n). It can be noticed from this table that W_R values (approximately 5.0) for thermal neutrons ($E_n < 0.1$ MeV) are about 4 times smaller than those (approximately 20) for fast neutrons ($E_n > 0.1$ MeV).

Taking into account that; (i) neutrons are produced from high-energy (>10 MV) accelerators, (ii) neutrons have significantly higher W_R than photons; and (iii) neutrons have a larger contribution to the dose delivered to distal normal organs/tissues during the prostate EBRT, it is therefore necessary to evaluate the dose from photons as well as neutrons in order to assess the risk of radiation-induced second malignancy resulted from prostate radiotherapy using a high-energy linear accelerator.

Table 6.1. *Neutron weighting factors (W_R) as a function of incident neutron energy (E_n) obtained using equation (6.1).*

Incident neutron energy (E_n) in MeV	Radiation weighting factor (W_R)	Incident neutron energy (E_n) in MeV	Radiation weighting factor (W_R)
1.0E-06	5.0	0.4	21.9
1.0E-05	5.0	0.5	22.0
1.0E-04	5.0	1.0	20.7
1.0E-03	5.0	2.0	17.3
5.0E-03	5.5	4.0	13.3
1.0E-02	6.3	6.0	11.1
5.0E-02	12.0	8.0	9.7
0.1	16.0	10.0	8.8
0.2	19.8	20.0	6.8
0.3	21.3	40.0	5.7

Neutrons are normally classified according to their energy because the type of reaction that a neutron undergoes depends very strongly on its energy (Cember 1996). Those neutrons whose energies exceed 0.1 MeV are called fast neutrons whilst thermal neutrons have the most probable energy at 0.025 eV and in the

region between thermal and fast, neutrons are considered intermediate, resonance, or slow neutrons (Cember 1996).

Distributions of out-of-field photons and neutrons produced from medical linacs have been reported previously. The radiation doses in these out-of-field locations around linac have been measured directly using variety of dosemeters or indirectly by simulation using computer codes. In the study of Vanhavere *et al* (2005), for example, peripheral neutron and photon doses in radiotherapy with an 18 MV accelerator were measured using BD-PND and BDT bubble detectors and LiF:Mg,Ti (TLD-700) TLDs respectively (results summarized in Table 7.1). The BD-PND detector is sensitive to fast neutrons (energy above 100 keV) only whilst the BDT detector primarily measures thermal neutrons. The TLD-700 TLDs are sensitive exclusively to photons. Kry *et al* (2005) measured out-of-field photons and neutrons independently using thermoluminescent dosimeters 700 (TLD-700) and moderated gold foil activation technique, respectively. Using the Rando phantom, out-of-field photon and neutron dose equivalents from step-and-shoot intensity-modulated radiation therapy (IMRT) at 10 anatomical sites in six organs were also determined in this study (results summarized in Table 7.1). Similarly, secondary neutron spectra and scattered photon dose from dynamic multileaf collimator (MLC) IMRT for 6 MV, 15 MV, and 18 MV beam energies were measured using gold-foil activation technique with the Bonner sphere and Harshaw TLD-700 in the study of Howell *et al* (2006) (see Table 7.1). Recently, Wang and Xu (2008) used the relative Metal Oxide Semiconductor Field Effect Transistor (MOSFET) dosemeters to measure non-target organ doses as the results of IMRT and 3D-CRT radiotherapy techniques (Table 7.1). MOSFET has an advantage over the passive

dosemeters such as TLDs and gold-foils used in the previous studies as it provides real-time reading. However, only photons can be measured using MOSFETs. Additional dosimeter is still required for neutron measurement.

From these studies, photons and neutrons were measured separately using different detectors and the organ doses especially from neutrons were estimated from the measured results. While TLDs are commonly used for photon dosimetry in most radiotherapy laboratories, the gold-foil and bubble detectors for neutron dosimetry are, in contrast, quite uncommon and may require a special technician and equipment to operate and analyze the results. Although the MOSFET detectors have been widely used in various medical applications (Wang & Xu 2008), their use is limited to photon dosimetry only. Therefore, there is a need to develop a simpler dosimetry technique based on single type dosimeter which can practically measure out-of-field photons and neutrons simultaneously.

In this thesis, direct measurement of out-of-field photons and neutrons produced by the 18 MV beam from a Varian iX medical linac was performed using pairs of glass-rod enriched ^{6}Li and ^{7}Li LiF:Mg,Cu,P TLDs. These TLDs have small dimensions with diameter of 2.0 mm and length of 12 mm. With a specially designed holder, several pairs of ^{6}Li (sensitive to neutrons and photons) and ^{7}Li (sensitive to photons only) LiF:Mg,Cu,P glass-rod TLDs can be put together to measure out-of-field photons and neutrons simultaneously. Normally, LiF:Mg,Cu,P is a material highly sensitive to radiation and it has been reported to be 23 – 35 times more sensitive than LiF:Mg,Ti (McKeever, 1995). Replacing natural Li with enriched ^{7}Li or ^{6}Li makes these detectors selectively more sensitive to photons and neutrons, respectively. TLD material containing ^{7}Li does not capture neutrons

because this isotope has very low neutron cross-section compared with that of ^{6}Li (Itoh *et al* 1993).

6.2 ^{6}LiF:Mg,Cu,P and ^{7}LiF:Mg,Cu,P glass-rod TLDs and calibrations

6.2.1 Enriched ^{6}Li and ^{7}Li LiF:Mg,Cu,P TLDs

To measure the out-of-field doses from photons and neutrons, glass-encased TLDs containing enriched ^{6}Li and ^{7}Li LiF:Mg,Cu,P TLD powder obtained from Gammasonics Institute for Medical Research, Australia, were used (Figure 6.3). General properties of both types of TLDs are presented in Table 6.2. Other common radiodosimetric characteristics of both types of TLDs are described in McKeever *et al* (1995). Generally, LiF:Mg,Cu,P (TLD-100H) with natural isotope of lithium (Li) contains 7.4% ^{6}Li and 92.6% ^{7}Li (Prahan 1989) and responds to both photons and neutrons. The response to neutrons is enhanced by enrichment of ^{6}Li which has high neutron cross-section of up to 942 barns at incident neutron energy (E_n) of 2.53 x 10^{-8} MeV (Tripathy *et al* 2009) in ^{6}LiF:Mg,Cu,P or suppressed by using lithium consisting entirely of ^{7}Li in ^{7}LiF:Mg,Cu,P (Obryk *et al* 2008) which has low neutron cross-section of 4.6 x 10^{-2} barns at the same incident neutron energy. ^{6}Li-enriched TLDs are highly sensitive to thermal neutrons via the neutron capture reaction, $n + {}^6Li \rightarrow \alpha(2.05\ MeV) + {}^3H(2.73\ MeV)$, whilst the sensitivity of ^{7}Li-enriched TLDs to thermal neutrons is almost negligible. In addition, both TLDs have a similar response to photons which can be determined by exposing these TLDs to the same radiation field. Cross-sections of ^{6}Li and ^{7}Li reactions to incident neutrons as a function of incident neutron energy are shown in Figure 6.4.

Figure 6.3. (Top) Enriched ^{6}LiF:Mg,Cu,P (clear colour) and ^{7}LiF:Mg,Cu,P (green colour) glass-rod TLDs obtained from Gammasonics Institute for Medical Research, Australia, (Bottom) TLD holder with cadmium filter installed.

Table 6.2. General properties of enriched ⁶LiF:Mg,Cu,P and ⁷LiF:Mg,Cu,P TLDs (Shanghai Renri Radiation Protection Equipment Co., Ltd.).

NOTE:
These images are included on page 177 of the print copy of the thesis held in the University of Adelaide Library.

Figure 6.4. Neutron reaction cross-sections for ⁶Li $(n + {}^6Li \rightarrow \alpha(2.05\ MeV) + {}^3H(2.73\ MeV))$ and ⁷Li (total neutron absorption) as a function of incident neutron energy (Nuclear Data Evaluation Lab, Korea Atomic Energy Research Institute, 2009).

TLDs are placed in specially designed holders (Figure 6.3, Right) provided with the purchase of TLDs. Eight pairs of ^{6}LiF:Mg,Cu,P (measures neutrons and photons) and ^{7}LiF:Mg,Cu,P (measures photons) TLDs are put inside the holder along with a cadmium filter to absorb thermal neutrons with energies below 0.5 eV (Figure 6.5). These TLDs must be used in pairs in order to be able to differentiate between the dose from photons and neutrons (method is described in section 6.3). The first 4 pairs are covered with a cadmium filter to measure radiation doses from photons and neutrons with energies above 0.5 eV. The last 4 pairs of TLDs are not covered with a cadmium filter to measure doses from photons and neutrons over the whole range of energies. The whole set of TLDs fully assembled, was originally designed for use as a personnel dosimeter to measure radiation doses from photons and neutrons including fast and thermal neutrons. This is important as the Relative Biological Effectiveness (RBE) of neutrons is energy dependent.

NOTE:
This figure is included on page 178 of the print copy of the thesis held in the University of Adelaide Library.

Figure 6.5. Total neutron cross-section of natural Cadmium (Nuclear Data Evaluation Lab, Korea Atomic Energy Research Institute, 2009).

6.2.1.1 Calibrations of ^{7}LiF:Mg,Cu,P glass-rod TLDs

Calibrations of ^{7}LiF:Mg,Cu,P glass-rod TLDs (35 in total) were carried out using the 18 MV beam from a Varian iX medical linear accelerator. These TLDs were placed in a perspex phantom and covered with RW3 (tissue substitute material with density of 1.045 g/cm³, PTW, Freiberg, Germany) build-up plates to ensure that they are located at the depth of maximum dose. Source-to-Skin Distance (SSD) of 100 cm and a field size of 10 x 10 cm² were used in measurement. Radiation dose of 1 Gy was delivered to the TLDs. Irradiated TLDs were left overnight at room temperature and read the following day. Finally, TLD samples were annealed, cooled and re-used.

To determine the sensitivity of ^{7}LiF:Mg,Cu,P TLDs, four separate irradiations of 1 Gy dose were given. Giving that $\overline{R^I_{7LiF}}$ is the average readout of all 35 ^{7}LiF:Mg,Cu,P glass-rod TLDs following an irradiation I, and $\overline{R_{7LiF}}$ is the average readout of all TLDs from all four irradiations, the normalized readout of any TLD ($^{norm}_x R_{7LiF}$) for an irradiation I is:

$$^{norm}_x R_{7LiF} = \left(\frac{_x R^I_{7LiF}}{\overline{R^I_{7LiF}}} \right) * \overline{R_{7LiF}} , \qquad (6.1)$$

where, $_x R^I_{7LiF}$ is the readout of a TLD number x for irradiation I, for example, $_1 R^1_{7LiF}$ is the readout of the TLD#1 for the 1st irradiation.

Then, the average normalized readout of a TLD# x for all four irradiations ($\overline{^{norm}_x R_{7LiF}}$) is:

$$\overline{^{norm}_{x}R_{7LiF}} = \frac{\sum_{I=1}^{4} {^{norm}_{x}R^{I}_{7LiF}}}{4}.$$ (6.2)

Finally, a sensitivity correction factor of a TLD# x (SCF_x) is determined using the following equation:

$$SCF_x = \overline{R_{7LiF}} \Big/ \overline{^{norm}_{x}R_{7LiF}}.$$ (6.3)

This factor represents the response of each ^{7}LiF:Mg,Cu,P TLD rod to photons relative to the whole TLD batch. This factor corrects for the variations in response of the TLDs to the same radiation dose as a result of variations in the amount of TLD powder contained within the glass rods.

In addition to SCF, a Batch Correction Factor (BCF) is also applied to the raw readouts to obtain TLD readouts corrected for batch response variations from one irradiation-reading-annealing cycle to another. To obtain BCF of ^{7}LiF:Mg,Cu,P TLDs, for example, four ^{7}LiF:Mg,Cu,P TLDs were selected at random. From the calibration of ^{7}LiF:Mg,Cu,P TLDs, the average normalized readout of these four selected TLDs was recomputed using equations (6.1) and (6.2). This newly obtained average normalized readout is now called "expected readout ($^{Expected}R_{7LiF}$)" of these four ^{7}LiF:Mg,Cu,P TLDs. For any further irradiations of ^{7}LiF:Mg,Cu,P TLDs, these four TLDs were separated from the whole batch and irradiated to 1 Gy calibration dose and average corrected readout ($\overline{^{Corr}R_{7LiF}}$) of these four TLDs was then calculated. This average corrected readout was then compared with the $^{Expected}R_{7LiF}$ to obtain BCF for a particular irradiation:

$$BCF = \frac{^{Expected}R_{7LiF}}{^{Corr}R_{7LiF}}. \qquad (6.4)$$

The BCF for irradiation of ^{6}LiF:Mg,Cu,P TLDs was also obtained using the same method as for ^{7}LiF:Mg,Cu,P TLDs. This BCF is applied, in addition to the SCF, to the raw readouts in order to correct the deviations in TLD readouts as a result of TLD response variation through multiple irradiation and annealing cycles.

The dose response linearity of ^{7}LiF:Mg,Cu,P TLDs was determined. This was done by delivering radiation doses of up to 6 Gy to the TLDs. The gross readout of each TLD was corrected using individual sensitivity and batch variation correction factors to obtain a corrected readout. Three irradiations were carried out and average values of corrected readouts were calculated. The dependence of the TLD readout on delivered dose was plotted.

Reproducibility of each ^{7}LiF:Mg,Cu,P TLD was also calculated as the ratio of standard deviation of mean (SDOM) and average corrected readout ($\overline{^{Corr}_{x}R_{7LiF}}$) of that particular TLD:

$$Reproducibility \ (\%) = \frac{SDOM}{^{Corr}_{x}R_{7LiF}}. \qquad (6.5)$$

TLD reading temperature profile was modified from that described in Oster *et al* (1993) and Bean-Amar *et al* (1999) in order to account for glass encasing. The following temperature setups were used in this study: pre-heating at 135°C for 45 seconds; and reading at 280°C for 120 seconds, the heating rate being kept constant at 2°C per second for both steps. Reading and annealing of TLDs were performed using Harshaw TLD 3500 Reader (Thermo Scientific, MA) and

Victoreen annealing oven (Model 2600-62-5, Victoreen Inc., OH). In the previous reports, a higher heating rate (10°C/s) and a shorter reading time were used but the TLDs were in the form of chips. For TLD chips, heat can be directly transferred to phosphor from the planchet using high heating rate and short reading time. However, lower heating rate (2°C/s) and longer readout (120 seconds) are needed for glass-rod TLDs to allow sufficient transfer of heat from planchet through glass into the powder contained inside the glass rod. Annealing of used TLDs was done in an oven at 240°C for 10 minutes (as recommended by the manufacturer) which is sufficient to eliminate any residual signals. Over-annealing could result in irreversible loss of TLD sensitivity (McKeever *et al* 1995). After annealing, TLDs were transferred to a copper tray and placed between copper blocks to rapid cool them to room temperature. This temperature treatment was applied to both ^{6}LiF:Mg,Cu,P and ^{7}LiF:Mg,Cu,P TLDs.

Finally, for ^{7}LiF:Mg,Cu,P TLDs, the ratio of average corrected readout ($\overline{^{Corr}R^{\gamma}_{7LiF}}$ in μC) calculated from every corrected readouts of ^{7}LiF:Mg,Cu,P TLDs to radiation dose (1 Gy) given to these TLDs was computed. This ratio ($\mu C/Gy$) will be used as readout-to-dose conversion factor to convert corrected readout of ^{7}LiF:Mg,Cu,P TLDs to photon dose.

6.2.1.2 Calibrations of ^{6}LiF:Mg,Cu,P glass-rod TLDs

Calibrations of ^{6}LiF:Mg,Cu,P glass-rod TLDs were also done using 18 MV X-ray beam from a Varian iX linac which produces both photons and neutrons at this energy. Hence, signals detected from these ^{6}LiF:Mg,Cu,P TLDs corresponded to both photons and neutrons. Identical setups as used for calibration of the

^{7}LiF:Mg,Cu,P TLDs were employed with the ^{6}LiF:Mg,Cu,P TLDs but radiation dose of 2 Gy was given instead to ensure that sufficient signals due to neutrons were generated by the TLDs (2 Gy was determined experimentally). Reading and annealing procedures of these TLDs were the same as those applied to the ^{7}LiF:Mg,Cu,P TLDs described previously. The same calculation procedures as ^{7}LiF:Mg,Cu,P TLDs for the sensitivity correction factor and reproducibility of ^{6}LiF:Mg,Cu,P TLDs were performed following three consecutive irradiations.

In order to obtain readout-to-neutron dose conversion factor, ^{6}LiF:Mg,Cu,P reading were cross-reference with CR-39 etch-track detectors readings for the same measurement conditions. The measurements were made at different locations in the patient plane. This would also provide the variation of doses as a function of distance from the isocentre. Preparation of TLD holders, measurement procedures, processing of irradiated TLDs and dose calculations were the same as described earlier. Up to 3 TLD holders were used at the same location for each measurement and up to 10 measurements were performed at each location to achieve sufficient statistical power. The dose given at the isocentre was 10 Gy using 18 MV X-ray beam, 10 x 10 cm^2 radiation field-size and 100 cm SSD. In addition, CR-39 etch-track detectors and (for some measurements only) AN/PDR-70 neutron survey meter were also placed at the same position as glass-rod TLDs to measure neutron doses. Determination of readout-to-dose (neutron) conversion factor for ^{6}LiF:Mg,Cu,P TLDs is described in section 6.3.

6.2.2 NRC RemRad AN/PDR-70 portable neutron survey meter

The AN/PDR-70 (Snoopy NP-2) portable neutron survey meter (Figure 6.6) made by Nuclear Research Corporation (Pennsylvania, USA) was placed in the same radiation field together with TLD holders containing the ^{6}LiF:Mg,Cu,P and ^{7}LiF:Mg,Cu,P TLD rods to measure neutron dose rate at 50 cm from the isocentre in the patient plane. The probe used in this survey meter is a proportional counter filled with boron-trifluoride (BF$_3$) gas with a high neutron cross section. The total cross section of B^{10} for neutrons of energy 0.253 eV (velocity = 2200 m/sec) is found to be 3,848 ± 38 barns (Schmitt *et al* 1960). The proportional counter is also surrounded by a boron-loaded attenuator and an inner and outer polyethylene moderator which slow down the neutrons to energies where they are efficiently captured by the nuclei of the detector gas (Moyers *et al* 2008).

The survey meter has been calibrated with the ^{246}Am/Be neutron source at the Australian Radiation Protection and Nuclear Safety Agency (ARPANSA), Melbourne, Australia. The latest calibration result was on October 10, 2006 with calibration factors of 10 or 13 μSv.hour^{-1}/mrem.hour^{-1} depends on the measuring positions (side-on or end-on) of the survey meter. All the measurements in this thesis using this neutron survey meter were performed with the end-on position, therefore, the latter calibration factor was used. With its built-in complex attenuator/moderator, this neutron survey meter provides true rem/hour (i.e. effective dose) reading independent of neutron energies in the range of 0.025 eV to 15 MeV and is also insensitive to gamma radiation of up to 500 Roentgens per hour (Nuclear Research Corporation, 1991). The response of this survey meter to

radiation was checked by putting the survey meter in the 6 MV X-ray beam radiation field. No reading was detected with the survey meter.

Figure 6.6. *A picture of AN/PDR-70 (Snoopy NP-2) portable neutron survey meter (Nuclear Research Corporation, Warrington, Pennsylvania, USA.) used in this study.*

6.2.3 CR-39 etch-track detector in Landauer® Luxel®+ dosimeter

The Landauer® Luxel®+ Ja type dosimeter (Figure 6.7) consists of an optically stimulated luminescence (OSL) detector based on aluminum oxide (Al_2O_3) and CR-39 etch-track detector based on allyl diglycol carbonate. The Al_2O_3 OSL detector is used to measure photon doses whilst CR-39 etch-track detector contains material which is insensitive to X-ray, beta or gamma radiations and thus it only detects fast neutrons (Landauer 2005). The fast neutrons are detected by using a polyethylene radiator that records recoil protons resulting from neutron interaction in the dosimeter. The range of neutron energies which can be detected by this detector is 40 keV to 40 MeV. In the current work, after exposure to radiations from a 18 MV X-ray beam, the dosimeter was sent back to the provider (Landauer, USA) for reading. During readout, the Al_2O_3 material is stimulated with selected frequencies of laser light causing material to illuminate in proportion to the amount of

radiation exposure. Meanwhile, the CR-39 detector is etched for 15 hours in chemical bath to enlarge exposure tracks and the fast neutron dose is determined by counting the nuclear tracks generated as a result of the proton recoils with the polyethylene radiator in the detector.

Figure 6.7. *A picture of the Landauer® Luxel®+ Ja type dosimeter. This dosimeter is normally used as a personnel dosimeter at the Royal Adelaide Hospital, South Australia. The rectangular part (yellow circle) is the CR-39 etch-track detector used for neutrons measurement.*

The average energy of neutrons produced from 18 MV medical linacs was found to range between 0.5 – 1.2 MeV which are classified as fast neutrons (Cember, 1996). As a result, the CR-39 etch-track detector was used to derive the readout-to-neutron dose conversion factor for ^{6}LiF:Mg,Cu,P TLDs. This was performed by placing the Ja type dosimeters containing CR-39 etch-track detectors at the same distance from isocentre as ^{6}LiF:Mg,Cu,P TLDs and delivering 10 Gy radiation dose.

In addition, another set of Ja type dosimeter was exposed to a calibrated ^{238}Pu/Be radioactive neutron source to verify the response of CR-39 etch-track detector to neutrons. The actual neutron output of this 3.15 Curies ^{238}Pu/Be source (0.89 x 10^7 neutrons/second) was verified a with rem meter previously (Ralston 1994) and the average neutron dose equivalent rate was found to be 90 ± 14 μSv/hour at 100 centimeters from the centre of the source. The AN/PDR-70 neutron survey meter

was also used to check the neutron dose rate from this source in the current work. The CR-39 was placed in the paraffin blocks setup in front of the neutron beam at 25 centimeters from the centre of the neutron source and irradiated for 23 hours. Measured neutron dose was compared with the calculated dose.

6.3 Measurements of out-of-field radiation doses

6.3.1 Out-of-field radiation doses at points-of-interest

In order to study out-of-field radiation doses, each TLD holder was filled with 2 pairs of each ^{6}LiF:Mg,Cu,P and ^{7}LiF:Mg,Cu,P TLDs (Figure 6.3, Bottom) and then placed on the treatment couch at the point-of-interest (50 centimeters from the isocentre in the superior-inferior direction in an isocentric plane). This point was selected because it is related to the location of lungs (which is a radiation sensitive organ) in the patient during prostate irradiation using EBRT techniques. The risk of second malignancy in the lungs associated with prostate radiotherapy has been identified in several reports, i.e. Movsas *et al* 1998, Brenner *et al* 2000, and Abdel-Wahab *et al* 2008. As a result, dose to lungs due to leakage and scattered radiations was investigated in the current work (Chapter 7).

The first (^{7}LiF:Mg,Cu,P) and second (^{6}LiF:Mg,Cu,P) pair of TLDs were covered with cadmium filter and readouts obtained from these TLDs were used to calculate fast neutron dose equivalents assuming that thermal neutrons (energies below 0.5 eV) were absorbed by cadmium filter. The third (^{7}LiF:Mg,Cu,P) and fourth (^{6}LiF:Mg,Cu,P) TLD pairs were not covered with cadmium filter (Figure 6.3). Hence, their reading results were used to calculate dose equivalents of neutrons (thermal + fast) and photons.

Initially, dependence of neutron dose rate as a function of the field size was investigated by delivering 1,000 monitor units (MU) to RW3 scattering plates using 18 MV beam and 100 cm Source-to-Skin Distance (SSD) with different radiation field-sizes. An AN/PDR-70 neutron survey meter was placed next to TLD holders to measure neutron dose rate during irradiation. The results of this measurement in terms of relative neutron dose rate compared to 10 x 10 cm^2 field-size were shown in Table 6.3. It can be noticed that the largest neutron reading was obtained for a field-size of 10 x 10 cm^2 at 50 centimeters from the isocentre in the patient plane. Consequently, 10 x 10 cm^2 field-size was used for subsequent measurements. This field size is also close to clinical setting for prostate irradiation.

***Table 6.3.** Relative neutron dose rate normalized to 10 x 10 cm^2 field-size as a function of radiation field-size (cm^2) measured with AN/PDR-70 neutron survey meter at 50 centimeters from the isocentre on the patient plane.*

Field-size (cm^2)	Relative neutron dose rate
2 x 2	0.95
5 x 5	0.95
10 x 10	1.0
15 x 15	1.0
20 x 20	1.0
30 x 30	0.8
40 x 40	0.8

6.3.1.1 Determination of ^{6}LiF:Mg,Cu,P TLDs readout due to neutron dose only

The following procedures were carried out to determine the corrected readouts of ^{6}LiF:Mg,Cu,P TLDs due to neutron dose only.

Initially, 8 randomly selected TLDs (4 each of ^{6}LiF:Mg,Cu,P and ^{7}LiF:Mg,Cu,P) were placed on a perspex plate and given a 2 Gy dose using 6 MV beam to be used as control TLDs providing a Batch Correction Factor (BCF) for each irradiation in subsequent measurements. Then, a ratio of the average corrected readout of the ^{7}LiF:Mg,Cu,P TLDs ($\overline{{}^{corr}R^\gamma_{7LiF}}$, in μC) to that of the ^{6}LiF:Mg,Cu,P TLDs ($\overline{{}^{corr}R^\gamma_{6LiF}}$, in μC) following 6 MV beam irradiation was calculated using equation (6.6) as shown below. The ratio represents the difference in response of ^{7}LiF:Mg,Cu,P TLDs to photons relative to ^{6}LiF:Mg,Cu,P TLDs (Gregori *et al* 2002):

$$k = \frac{\overline{{}^{corr}R^\gamma_{7LiF}}}{\overline{{}^{corr}R^\gamma_{6LiF}}} \ . \tag{6.6}$$

For ^{6}LiF:Mg,Cu,P TLDs placed at 50 centimeters from the isocentre, their raw readouts ($R^{n+\gamma}_{6LiF}$, in μC) as a result of 10 Gy dose irradiation to RW3 scattering plates using 18 MV X-ray beam from Varian iX linear accelerator were corrected for background readings, SCF and BCF to obtain corrected readouts corresponding to photon and neutron doses ($^{Corr}R^{n+\gamma}_{6LiF}$, in μC).

Finally, the corrected readout of ^{6}LiF:Mg,Cu,P TLDs due to neutron dose only ($^{Corr}R^n_{6LiF}$, in μC) can be obtained from the corrected readout of ^{6}LiF:Mg,Cu,P TLDs

due to neutron and photon doses ($^{Corr}R_{6LiF}^{n+\gamma}$, in μC) using the k factor derived from equation (6.6) and the following equation:

$$^{corr}R_{6LiF}^{n} = \left[\left(R_{6LiF}^{n+\gamma} - B.G. \right) * SCF * BCF \right] - \left| \frac{^{corr}R_{7LiF}^{\gamma}}{k} \right|. \qquad (6.7)$$

6.3.1.2 Determination of ⁶LiF:Mg,Cu,P TLD corrected readout due to total and fast neutrons

$^{Corr}R_{6LiF}^{\gamma+n}$ is the corrected readout of a ⁶LiF:Mg,Cu,P TLD corresponding to photon and neutron doses (2ⁿᵈ column, Table 6.6) and $^{Corr}R_{7LiF}^{\gamma}$ is the corrected readout of a ⁷LiF:Mg,Cu,P TLD as a result of photon dose only (3ʳᵈ column, Table 6.6) in the holder without cadmium filter. Therefore, the corrected readout of a ⁶LiF:Mg,Cu,P TLD as a result of (total) neutron dose ($^{Corr}R_{6LiF}^{n_{total}}$) (6ᵗʰ column, Table 6.6) is:

$$^{Corr}R_{6LiF}^{n_{total}} = {}^{Corr}R_{6LiF}^{\gamma+n} - \frac{^{Corr}R_{7LiF}^{\gamma}}{k}, \qquad (6.8)$$

where k is the ratio represents the difference in response of ⁷LiF:Mg,Cu,P TLDs to photons relative to ⁶LiF:Mg,Cu,P TLDs (equation 6.6).

As discussed earlier, the cadmium filter absorbs neutrons with energies below 0.5 eV, therefore, the corrected readout of a ⁶LiF:Mg,Cu,P TLD in the holder with cadmium filter ($^{Corr}_{Cd}R_{6LiF}^{\gamma+n_{fast}}$) represents the response of this ⁶LiF:Mg,Cu,P TLD to photon and fast neutron irradiations (e.g. fourth column, Table 6.6). In addition, $^{Corr}_{Cd}R_{7LiF}^{\gamma}$ is the corrected readout of a ⁷LiF:Mg,Cu,P TLD with cadmium filter due to photon dose (e.g. fifth column, Table 6.6). Therefore, the corrected readout of a ⁶LiF:Mg,Cu,P TLD as a result of fast neutron dose ($^{Corr}_{Cd}R_{6LiF}^{n_{fast}}$) only is:

$$^{Corr}_{Cd}R^{n_{fast}}_{6LiF} = {}^{Corr}_{Cd}R^{\gamma+n_{fast}}_{6LiF} - \frac{{}^{Corr}_{Cd}R^{\gamma}_{7LiF}}{k}. \tag{6.9}$$

6.3.1.3 Determination of readout-to-neutron dose conversion factor for ^{6}LiF:Mg,Cu,P TLDs

In order to derive a readout-to-neutron dose conversion factor for ^{6}LiF:Mg,Cu,P TLDs, two CR-39 etch-track detectors were placed at 15, 30, 50, 75, and 100 centimeters back from the isocentre together with ^{6}LiF:Mg,Cu,P TLDs to observe the variation of neutron dose a function of distance from the isocentre and to obtain the calibration curve. The irradiation setup for CR-39 detectors was the same as used with TLDs. The results from these measurements, in terms of ratio of fast neutron dose equivalent (mSv) obtained with CR-39 detectors and corrected readout of ^{6}LiF:Mg,Cu,P TLDs (μC) due to fast neutron dose only, were used to derive the readout-to-neutron dose conversion factors for ^{6}LiF:Mg,Cu,P TLDs: i.e. to obtain the neutron dose equivalent, ${}^{corr}R^{n}_{6LiF}$ (in μC) calculated from equation (6.5) was converted to dose by cross-referencing to neutron dose equivalent (mSv) measured with the CR-39 etch-track detectors. In other words, the neutron dose equivalent (H_n, in mSv) of the CR-39 etch-track detectors can be directly correlated to $\overline{{}^{corr}R^{n}_{6LiF}}$ (the average corrected readout from all measurements) providing a readout-to-neutron dose conversion factor (mSv/μC).

6.4. Results

6.4.1 Calibration results of [7]LiF:Mg,Cu,P TLDs

In total, 35 [7]LiF:Mg,Cu,P TLD rods were calibrated. The amount of TLD phosphor in each rod is not exactly equal and this affects their sensitivity/response to radiation dose. The average normalized readout of each [7]LiF:Mg,Cu,P rod ($\overline{^{norm}R^{\gamma}_{7LiF}}$), standard deviation (S.D), reproducibility and sensitivity correction factor (SCF) are shown in Table 6.4. Following up to 4 irradiations using 1 Gy dose using 18 MV X-ray beam, an average readout obtained with Harshaw 3500 TLD Reader for the whole batch of these TLDs was approximately 22.4 ± 1 μC. Figure 6.8 shows the typical glow-curve of [7]LiF:Mg,Cu,P TLD rod following 1 Gy dose irradiation. A plot showing average normalized readout of each TLD and average readout of the whole batch is shown in Figure 6.9.
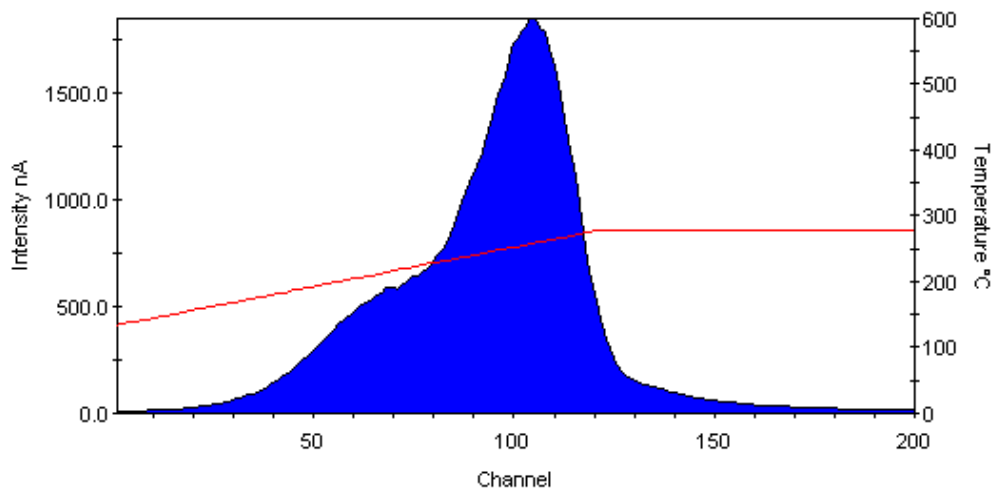

Figure 6.8. *A typical glow-curve of [7]LiF:Mg,Cu,P TLDs resulting from 1 Gy photon dose irradiation using 18 MV beam from Varian iX medical linear accelerator. The signal was obtained using Harshaw 3500 TLD Reader and analyzed with WinREM software.*
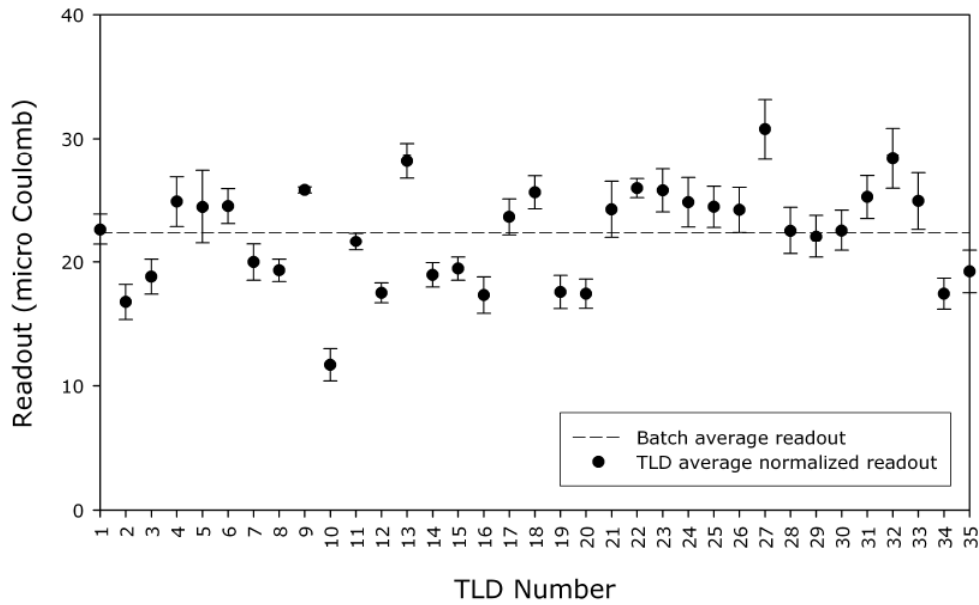
Figure 6.9. *A plot showing average normalized readout of each ^{7}LiF:Mg,Cu,P TLD (•) and average readout of the whole batch (dash line).*

Table 6.4. *Calibration results of ^{7}LiF:Mg,Cu,P TLD rods using 1 Gy photons dose using 18 MV X-ray beam from Varian iX medical linac (10 x 10 cm^2 FS, 100 cm SSD).*

TLD#	$\overline{^{norm}R^\gamma_{7LiF}}$ in μC	Standard Deviation (S.D) in μC	Reproducibility (%)	Sensitivity Correction Factor (SCF)
1	22.7	1.3	2.8	0.9892
2	16.8	1.4	4.2	1.3386
3	18.5	1.4	4.4	1.1936
4	25.0	2.0	4.0	0.8996
5	24.3	3.0	7.0	0.9156
6	24.6	1.4	2.9	0.9129
7	20.0	1.5	3.7	1.1230
8	19.3	0.9	2.3	1.1625
9	26.0	0.2	0.5	0.8667
10	11.7	1.3	5.5	1.9193
11	21.3	0.7	1.9	1.0349
12	17.7	0.8	3.2	1.2826
13	28.2	1.4	2.5	0.7950
14	18.8	1.0	3.0	1.1843
15	19.4	0.9	2.4	1.1533
16	17.2	1.5	5.0	1.2959

Table 6.4. *Continued.*

TLD#	$\overline{^{norm}R^{\gamma}_{7LiF}}$ in μC	Standard Deviation (S.D) in μC	Reproducibility (%)	Sensitivity Correction Factor (SCF)
17	23.5	1.5	3.6	0.9461
18	25.7	1.3	3.0	0.8731
19	17.6	1.3	3.8	1.2773
20	17.7	1.2	3.8	1.2876
21	24.3	2.3	4.7	0.9225
22	26.0	0.8	1.5	0.8618
23	25.6	1.7	3.9	0.8677
24	24.9	2.0	4.0	0.9013
25	24.5	1.7	3.4	0.9150
26	24.5	1.8	4.3	0.9243
27	30.7	2.4	3.9	0.7292
28	22.6	1.9	4.2	0.9938
29	21.9	1.7	4.6	1.0147
30	22.6	1.7	3.7	0.9927
31	25.3	1.7	3.4	0.8861
32	28.4	2.4	4.2	0.7892
33	25.0	2.3	4.6	0.8976
34	17.3	1.3	4.2	1.2875
35	19.2	1.7	4.4	1.1678

For the same dose and irradiation conditions, response of all the ^{7}LiF:Mg,Cu,P TLDs was within about ± 30% of the average readout of the whole batch except TLD#10 with response almost 50% lower than the average. In comparison to other TLDs, this TLD visually appeared to contain much less TLD powder. To compensate any over- or under-response of the individual ^{7}LiF:Mg,Cu,P TLDs to X-rays, the corresponding sensitivity correction factor was applied to the raw readout of each individual TLD rod. The mean reproducibility of these TLD rods was 3.6 ± 1.2% with most TLDs having reproducibility within 5% and only two TLDs (#5 and #10) exceeded this value.

Figure 6.10 shows the dose-response curve of [7]LiF:Mg,Cu,P TLD rods. It was found that the response was linear within the range of doses used in this calibration (up to 6 Gy). The manufacturer of these TLDs claimed that their response to photons was linear to dose up to 12 Gy. The full range was not investigated in the current work because the dose beyond 6 Gy was not expected for out-of-field measurements.

In summary, the average corrected readout of [7]LiF:Mg,Cu,P TLDs corresponding to 1 Gy irradiation dose was 22.4 μC. Therefore, the readout-to-dose conversion factor of [7]LiF:Mg,Cu,P TLDs for X-ray exposures is 22.4 $\mu C/Gy$ or 44.6 $mSv/\mu C$ in terms of photon dose equivalent providing that the radiation weighting factor for X-rays is 1.0 (ICRP Publication 60, 1991).
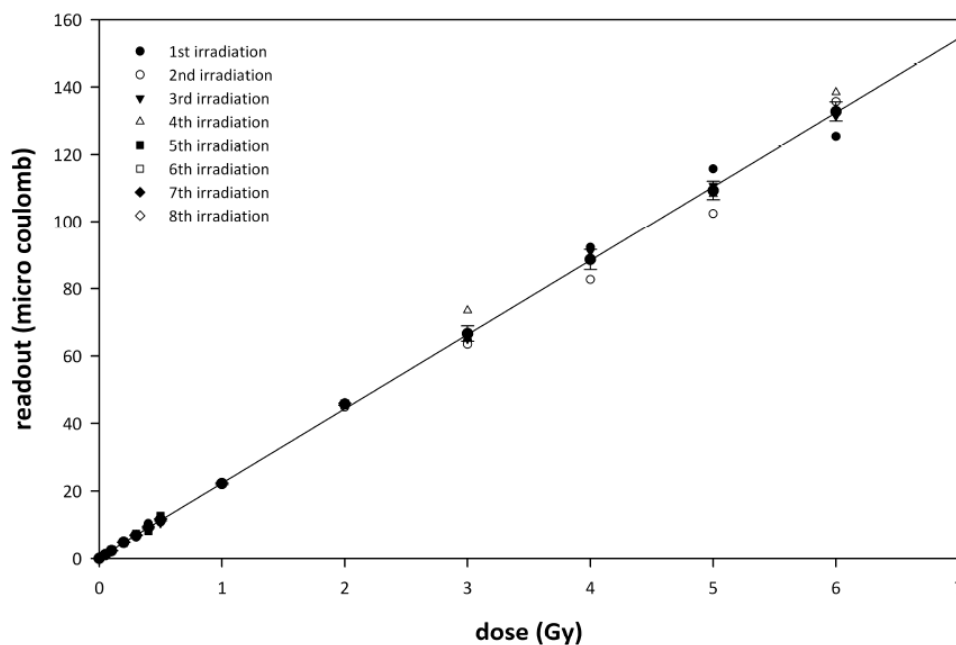

Figure 6.10. *Dose-response linearity of [7]LiF:Mg,Cu,P TLD rods irradiated to X-ray doses of up to 6 Gy using 18 MV beam from Varian iX linear accelerator.*

6.4.2 Calibration results of ^{6}LiF:Mg,Cu,P TLDs

The average normalized readouts ($\overline{^{norm}R_{6LiF}^{n+\gamma}}$), S.D, SCF, and reproducibility values as well as the typical glow curve of ^{6}LiF:Mg,Cu,P TLDs are shown in Table 6.5 and Figure 6.11 respectively. The corresponding average readout was 38.8 ± 4 μC. The average normalized readout for most of ^{6}LiF:Mg,Cu,P TLDs was well within ±1 S.D of the batch average readout (Figure 6.12) whilst those of TLD numbers 4, 9, and 15 were within ±2 S.D. The mean reproducibility for this group of TLDs was 3.5 ± 2.2%.

Table 6.5. *Calibration results of ^{6}LiF:Mg,Cu,P TLD rods using 2 Gy dose using 18 MV X-ray beam from Varian iX linear accelerator (10 x 10 cm² FS, 100 cm SSD).*

TLD #	$\overline{^{norm}R_{6LiF}^{n+\gamma}}$ in μC	Standard Deviation (S.D) in μC	Reproducibility (%)	Sensitivity Correction Factor (SCF)
1	36.4	0.1	0.2	1.0652
2	38.2	2.4	3.6	1.0146
4	31.2	1.3	2.4	1.2409
5	34.7	4.9	7.4	1.1177
6	43.2	2.2	3.3	0.8986
8	40.3	3.9	7.1	0.9614
9	48.0	2.0	3.6	0.8073
10	43.6	1.0	1.5	0.8889
11	38.5	1.1	1.7	1.0061
12	39.2	3.3	6.1	0.9880
13	41.2	1.0	1.5	0.9415
14	42.2	2.4	3.5	0.9184
15	31.5	4.1	6.2	1.2308
16	35.7	2.5	3.8	1.0876
17	37.8	0.2	0.4	1.0274
19	42.0	0.8	1.1	0.9230
20	35.6	0.8	1.3	1.0885

Table 6.5. Continued.

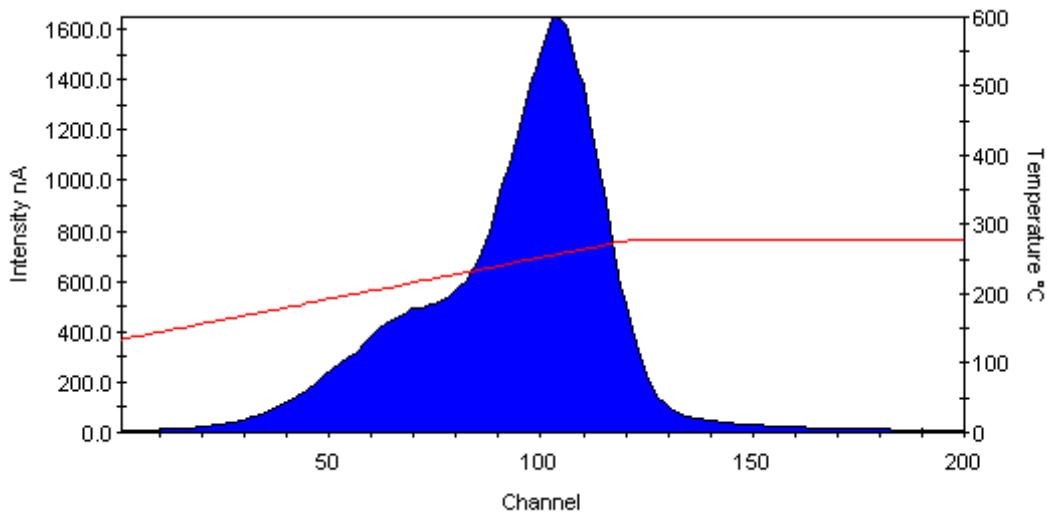| TLD #	$\overline{^{norm}R^{n+\gamma}_{6LiF}}$ in μC	Standard Deviation (S.D) in μC	Reproducibility (%)	Sensitivity Correction Factor (SCF)
21	42.3	3.8	5.6	0.9163
22	37.1	3.1	4.6	1.0444
24	38.8	1.0	1.5	0.9984
25	39.1	0.8	1.2	0.9924
26	34.3	0.8	1.2	1.1319
27	33.8	1.9	2.8	1.1457
28	37.3	1.9	2.8	1.0400
30	34.1	4.9	7.2	1.1369
31	43.1	3.9	5.8	0.8999
32	41.3	3.8	5.7	0.9383
33	44.4	3.3	4.9	0.8740

Figure 6.11. *A typical glow-curve of ^{6}LiF:Mg,Cu,P TLD rods following 2 Gy photon doses irradiation using 18 MV X-ray beam from Varian iX linear accelerator. The signal was obtained using Harshaw 3500 TLD Reader and analyzed with WinREM software.*
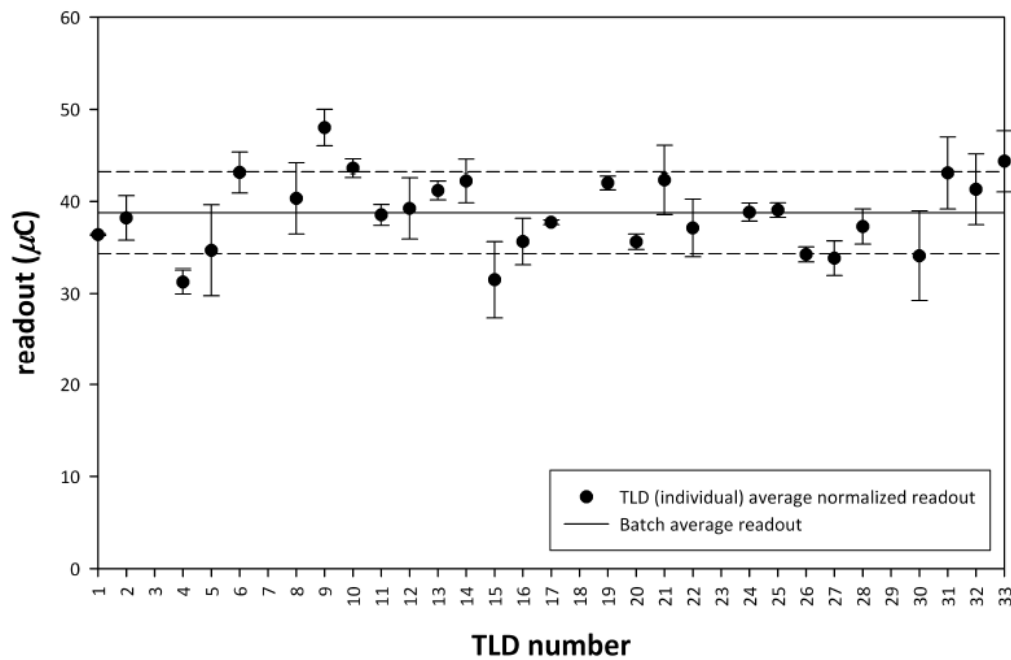
Figure 6.12. *A plot showing average normalized readout of each ^{6}LiF:Mg,Cu,P TLD (•) and average readout of the whole batch (——). The above and below broken lines represent batch average readout plus and minus 1 S.D respectively.*

6.4.3 Readout-to-neutron dose conversion factor for ^{6}LiF:Mg,Cu,P TLDs using CR-39 etch-track detectors

The results of Luxel®+ Ja type dosimeters and ^{6}LiF:Mg,Cu,P TLDs corrected readouts corresponding to exposures at various distances from the beam central axis as a result of 10 Gy radiation dose to the isocentre are shown in Table 6.6. For 6 MV X-ray beam, only one measurement with CR-39 detector was made at 50 centimeters distance from the isocentre.

Table 6.6. *Fast neutron and photon dose equivalents (mSv) obtained with Luxel® Ja Type dosimeters and corrected readouts of ^{6}LiF:Mg,Cu,P TLDs corresponding to 10 Gy dose irradiation using 6 &18 MV X-ray beams from Varian iX linear accelerator.*

Distance from the isocentre (cm)	Fast neutron dose equivalent (mSv) ± S.D	Photon dose equivalent (mSv) ± S.D	Corrected readout due to fast neutron exposure (μC) ± S.D	Ratio (mSv/μC)
-- 6 MV X-ray beam --				
50	0.0	13.5	Not detectable	–
-- 18 MV X-ray beam --				
15	27.5 ± 1.9	–	1.7 ± 1.4	16.2
30	23.0 ± 3.5	–	0.5 ± 0.4	50.8
50	17.8 ± 1.1	–	0.1 ± 0.1	175.7
75	12.8 ± 1.2	–	0.1 ± 0.1	125.6
100	10.6 ± 1.1	–	0.1 ± 0.1	110.3

The results shown in Table 6.6 confirmed that there were no out-of-field neutrons produced and/or detected for a 6 MV X-ray beam. When 18 MV beam was used out-of-field neutrons were detected with the CR-39 etch-track detectors.

A CR-39 detector was also irradiated to neutrons from a calibrated ^{238}Pu/Be neutron source to verify the accuracy of its neutron dose response. At the measuring distance of approximately 25 centimeters from the source, the calculated neutron dose rate was 1.44 ± 0.2 mSv/hour and the dose rate measured with the AN/PDR-70 neutron survey meter was 1.5 mSv/hour. According to these dose rates, the corresponding neutron dose equivalents at this distance after 23

hour exposure were 33.1 ± 4.6 mSv and 34.5 mSv for calculated and measured dose rates respectively. The neutron dose equivalent measured with CR-39 etch-track detector placed at the same distance after 23 hour exposure was 30.0 mSv which agreed well with both calculated and measured dose rates. Therefore, it is possible to use the CR-39 etch-track detector as a cross-reference to derive the readout-to-neutron dose conversion factor for ^{6}LiF:Mg,Cu,P TLDs.

The fast neutron dose equivalents measured with the CR-39 etch-track detectors and corrected readouts of ^{6}LiF:Mg,Cu,P TLDs (μC) due to neutrons exposure only as well as the ratio of these two numbers at different distances from the isocentre are also shown in Table 6.6. Figure 6.13 shows a curve of measured fast neutron dose equivalent using CR-39 detectors to the corrected readout due to fast neutron only from ^{6}LiF:Mg,Cu,P TLDs ratio as a function of distance from the isocentre.

It can be noticed that the neutron dose equivalent decreases with increasing distance from the isocentre. In addition, the last column of Table 6.7 and Figure 6.13 show that the ratio of neutron dose equivalent measured by CR-39 etch-track detector and the corrected readout due to fast neutron exposure only of ^{6}LiF:Mg,Cu,P TLDs changes as a function of distance from the isocentre. As a result, the readout-to-neutron dose conversion factor corresponding to a given distance (from isocentre) of a particular measurement should be used for dose assessments. Therefore, the curve shown in Figure 6.13 will be used as a calibration curve for ^{6}LiF:Mg,Cu,P TLDs to obtain the conversion factor to convert the TLDs' corrected readout to neutron dose equivalent.
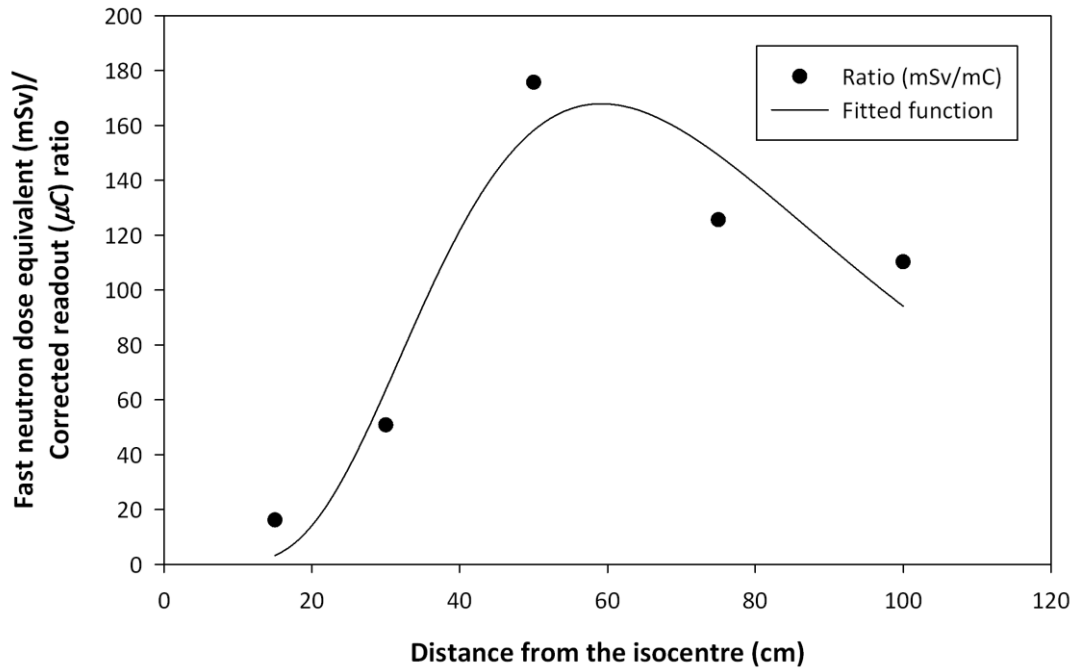
Figure 6.13. *A plot shows the ratio of measured fast neutron dose equivalents (mSv) from CR-39 etch-track detector to corrected readouts (μC) of ^{6}LiF:Mg,Cu,P TLDs due to fast neutron exposure as a function of distance (cm) from the isocentre.*

6.4.4 Out-of-field radiations measurements

Table 6.7 shows the average corrected readouts of ^{6}LiF:Mg,Cu,P and ^{7}LiF:Mg,Cu,P TLD pairs as well as the average corrected readouts due to total and fast neutrons and due to photon exposure only in a mixed-radiation field located 50 centimeters from the isocentre resulting from 10 Gy radiation dose to the isocentre. The results were obtained from 5 measurements. The corrected readouts due to total and fast neutron exposures were obtained using equations (6.8) and (6.9) as described earlier in section 6.3.1.2. The values of *k* factor observed in 5 measurements were ranging from 1.11 to 1.22. Providing that value of *k* factor represents the response of ^{7}LiF:Mg,Cu,P TLDs to photon compared to ^{6}LiF:Mg,Cu,P TLDs, as a result,

^{7}LiF:Mg,Cu,P TLDs have around 10 – 20% higher sensitivity to megavoltage photons compared to ^{6}LiF:Mg,Cu,P TLDs.

Table 6.7. *Average corrected TLD readout (μC) of ^{6}LiF:Mg,Cu,P and ^{7}LiF:Mg,Cu,P TLDs in each TLD holder located at 50 cm from the isocentre corresponding to 10 Gy irradiation dose using 18 MV X-ray beam from Varian iX linear accelerator.*

TLD Holder#	Average corrected TLD readouts (μC) ± S.D				Average corrected readout due to total neutrons (μC) ± S.D	Average corrected readout due to fast neutrons (μC) ± S.D	Average corrected readout due to photons (μC) ± S.D
	Without Cd filter (total neutrons + photons)		With Cd filter (fast neutrons + photons)				
	^{6}LiF:Mg,Cu,P	^{7}LiF:Mg,Cu,P	^{6}LiF:Mg,Cu,P	^{7}LiF:Mg,Cu,P			
1	0.67 ± 0.4	0.61 ± 0.5	0.47 ± 0.2	0.46 ± 0.3	0.15 ± 0.1	0.08 ± 0.1	0.54 ± 0.4
2	0.66 ± 0.3	0.67 ± 0.4	0.51 ± 0.2	0.52 ± 0.3	0.08 ± 0.1	0.08 ± 0.1	0.59 ± 0.4
3	0.77 ± 0.4	0.77 ± 0.5	0.54 ± 0.2	0.58 ± 0.3	0.10 ± 0.1	0.06 ± 0.1	0.67 ± 0.4
4	0.69 ± 0.4	0.72 ± 0.6	0.52 ± 0.3	0.50 ± 0.4	0.08 ± 0.1	0.09 ± 0.1	0.61 ± 0.5
5	0.62 ± 0.4	0.68 ± 0.6	0.45 ± 0.2	0.50 ± 0.4	0.07 ± 0.1	0.06 ± 0.1	0.59 ± 0.5
6	0.81 ± 0.5	0.79 ± 0.7	0.58 ± 0.36	0.57 ± 0.5	0.15 ± 0.2	0.14 ± 0.1	0.68 ± 0.5
average	*0.69 ± 0.4*	*0.70 ± 0.5*	*0.51 ± 0.2*	*0.52 ± 0.4*	*0.10 ± 0.1*	*0.09 ± 0.1*	*0.60 ± 0.4*

The standard deviation (S.D) shown in this as well as other tables were calculated using a following formalism:

$$S.D = \sqrt{\sum_{i}^{n}\left(x_i - \overline{X}\right)^2 \Big/ n}, \qquad (6.10)$$

where x_i is the corrected readout, $\overline{X}$ is the average corrected readout, and n is the number of data points used in the calculation.

The results shown in Table 6.7 show a specific case of measurements performed at 50 centimeters distance from the beam axis. One finding from this measurement is that it is possible to differentiate fast neutron readout from that of thermal neutrons by using cadmium filter to absorb neutrons with energies below 0.5 eV. The differences in readouts obtained using [6]LiF:Mg,Cu,P TLDs with cadmium filter and those without cadmium filter correspond to thermal neutrons.

Table 6.8 shows neutron and photon dose equivalents measured using [6]LiF:Mg,Cu,P and [7]LiF:Mg,Cu,P glass-rod TLDs at different locations in the patient plane corresponding to 10 Gy radiation dose at the isocentre using 18 MV X-ray beam from Varian iX linac with 10 x 10 cm[2] radiation field-size and 100 cm SSD. For photon dose equivalent, the readout-to-photon dose conversion factor of 44.6 $mSv/\mu C$ was applied to [7]LiF:Mg,Cu,P TLDs corrected readouts whilst corresponding conversion factors depending on the distance from the isocentre (Table 6.7 an Figure 6.13) were applied to the corrected readouts of [6]LiF:Mg,Cu,P TLDs to obtain (total and fast) neutron dose equivalents. The thermal neutron dose equivalents shown in Table 6.8 were derived as the difference between total and fast neutron dose equivalents. However, as discussed earlier in section 6.1 and according to neutron W_R data shown in Table 6.1, the radiation weighting factors for neutrons with energies below 0.1 MeV are approximately 5 whilst those for fast neutrons are approximately 20. As a result, the thermal neutron readouts (μC) were obtained as the difference of the total and fast neutron readouts (μC). The same calibration factor was applied to thermal neutron readouts as for the fast neutrons and then divided by 4 to account for W_R.

Table 6.8*. Ambient (in-air) photon and neutron dose equivalents (µSv) per MU measured with ⁶LiF:Mg,Cu,P and ⁷LiF:Mg,Cu,P glass-rod TLDs, and CR-39 etch-track detector at different distances from isocentre in the patient plane corresponding to 10 Gy X-rays dose irradiation using 18 MV X-ray beam from Varian iX linear accelerator.*

Distance from isocentre (cm)	Neutron dose equivalent (μSv) per MU ± S.D			Photon dose equivalent (μSv) per MU ± S.D	Neutron (total)/ photon dose equivalents ratio	Total neutron dose equivalent per 1 Gy target dose (mSv)
	Total	Fast	Thermal			
15	27.4 ± 39.9	59.1 ± 49.9	3.1 ± 7.2	215.5 ± 94.6	0.1	2.7
30	9.9 ± 10.4	23.0 ± 19.4	0.6 ± 1.3	56.3 ± 19.0	0.2	1.0
50	17.8 ± 20.5	15.4 ± 14.9	2.2 ± 4.9	26.7 ± 18.7	0.7	1.8
75	7.8 ± 3.8	12.7 ± 4.5	0.1 ± 0.3	2.7 ± 0.6	2.9	0.8
100	7.4 ± 3.0	10.6 ± 3.8	0.1 ± 0.1	1.5 ± 0.4	4.9	0.7

It can be noticed from these results that both photon and neutron in-air dose equivalents were the highest close to the isocentre and the doses decreased with increasing distance from the isocentre. At 50 centimeters and further from the isocentre the photon dose equivalents decreased exponentially whilst the neutron dose equivalents were constant for distances of up to 100 centimeters. This resulted in the increasing of the total neutron/photon Dose Equivalent Ratio (DER) from 0.7 at 50 centimeters to 2.9 and 4.9 at 75 and 100 centimeters, respectively. The distributions of photon and neutron dose equivalents as a function of distance observed in this study were similar to other published data (Ongaro *et al* 2000 and Vanhavere *et al* 2004).

6.5 Discussion

Measurement of out-of-field neutron and photon doses in the accelerator based radiotherapy has become an important issue since linacs operating at high-energies (>10 MV) produce secondary radiations which irradiate parts of patient's anatomy distal to the target region. This radiation dose contributes towards induction of second primary cancer in normal tissues outside the treated area. A pair of ^{6}LiF:Mg,Cu,P and ^{7}LiF:Mg,Cu,P TLD rods without cadmium filter can be used to determine radiation doses from photons and (fast and thermal) neutrons in a mixed-radiation field. The addition of cadmium filters which absorbs neutrons with energy below 0.5 eV, enables the dose contribution from thermal neutrons to be differentiated from that contributed by fast neutrons.

Theoretically, the response of LiF:Mg,Cu,P material to radiation dose is linear. The range of linearity extends from approximately 0.3 mR up to 1000 R (McKeever, 1995). In this study, for the ^{7}LiF:Mg,Cu,P TLD rods, the range of dose-response linearity extended up to the photon doses of 6 Gy. Investigation of linearity at higher doses was not performed because out-of-field photon doses are not expected to exceed this calibration dose-range. Variations in dose-response of ^{7}LiF:Mg,Cu,P TLD rods to the same photon dose were observed. Visually, differences in phosphor content among TLD rods can be seen and these affect the radiation sensitivity of an individual TLD rod. However, this variation was corrected for by applying a sensitivity correction factor individually to raw readout of each TLD rod. Additionally, a batch correction factor obtained from the control TLDs was also applied to the raw readouts to correct for variations corresponding

to changes in ambient irradiation conditions and TLD behavior as a result of multiple irradiation-reading-annealing cycles.

The calibrations performed in this study suit our needs in the way that neutron dose measurement can be made in the mixed-radiation field where photons are dominant. However, in order to convert the ^{6}LiF:Mg,Cu,P TLD readouts into equivalent dose, a calibrated secondary passive neutron dosimeter is needed to cross-calibrate with the TLDs. In this case, CR-39 etch-track detectors were used. This detector is sensitive to wide-range (40 keV – 40 MeV , Landauer 2005) of fast neutrons which are the main neutrons produced from high-energy linear accelerators (Figure 6.1, Lin *et al* 2001, Huang *et al* 2005, Facure *et al* 2005, and Howell *et al* 2006). The response of CR-39 etch-track detector to neutrons was also verified by irradiation of CR-39 detector with a known calibrated neutron source (^{238}Pu/Be) and the neutron dose equivalent obtained with this detector was well within the range of calculated and measured dose equivalent values. Using the CR-39 etch-track detector neutron dose equivalents (mSv) and corrected readout (μC) of ^{6}LiF:Mg,Cu,P TLDs due to neutron exposure only, the readout-to-neutron dose conversion factor (mSv/μC) for a specific measuring distance (from the isocentre) was derived and applied to the readouts of ^{6}LiF:Mg,Cu,P TLDs to obtain neutron dose equivalents.

The cross-calibration method based on neutron doses measured with the CR-39 etch-track detector employed in this study may not replace a standard calibration method based on TLD irradiation using standardized neutron source such as Am/Be or Pu/Be. However, a problem may also arise when calibration against these standard sources is performed as they emit fast neutrons only. The mean

neutron energy produced by ^{238}Pu/Be and ^{241}Am/Be is 4.5 MeV and 4.4 MeV respectively (Mayer *et al* 2004 and Tripathy *et al* 2009) whilst neutrons produced from high-energy linear accelerators peak around 1 MeV with the most probable neutron energy at 0.5 MeV (Facure *et al* 2005). Therefore, there might be benefits in calibrating TLDs against the true linear accelerator neutron spectrum. It was shown in the current work that out-of-field neutron dose equivalents measured using ^{6}LiF:Mg,Cu,P TLDs calibrated against CR-39 etch-track detector were within the range reported in the literature. Accordingly, even without a standardized neutron source, calibration of ^{6}LiF:Mg,Cu,P TLDs for neutron measurements can be done using the method of cross-calibration with the CR-39 etch-track detector.

The neutron doses from 18 MV medical linacs have been found to vary between different machines and radiation therapy techniques. Regardless of techniques and type of accelerator machine, the neutron dose equivalent per unit photon dose ranges from as low as 0.1 mSv/Gy up to 20.4 mSv/Gy (Jaradat 2008 and Chibani 2003). Using pairs of ^{6}LiF:Mg,Cu,P and ^{7}LiF:Mg,Cu,P TLDs and cross-calibration with the CR-39 etch-track detector, the range of total ambient neutron (fast + thermal) dose equivalent per 1 Gy target dose observed in this study (0.7 – 2.7 mSv/Gy) was found to be within the reported range with estimated neutron dose equivalent of 1.8 mSv/Gy at 50 centimeters from the isocentre was comparable to other reports at the same accelerator energy (Liu *et al* 1997, d'Errico *et al* 1998, Ongaro *et al* 2000, and Zanini *et al* 2004). It has also been reported that the neutron dose equivalent lies between 1 and 4.8 mSv/Gy, depending on accelerator characteristics and distance from the isocentre (Ongaro *et al* 2000).

High variations in measured photon and neutron doses have been observed in the current work. These variations in results either of photon or neutron dose equivalents are related to several factors such as directional variations of the dose distributions, statistical variations in production of secondary photons and neutrons originated from random interactions in the head of a linear accelerator, uncertainty of the CR-39 etch-track detector used for cross-calibration as well as energy dependence in ^{6}LiF:Mg,Cu,P (±50% for E_n from thermal to 20 MeV) TLDs. Variations caused by the intrinsic uncertainty of both TLD types were reduced by applying individual sensitivity and (the whole) batch correction factors. It can be noticed though that the doses measured by both ^{6}LiF:Mg,Cu,P and ^{7}LiF:Mg,Cu,P TLDs were generally small (μSv or mSv) especially at further distances from the isocentre. These small doses correspond to very small readout signals (μC) of ^{6}LiF:Mg,Cu,P TLDs resulting in large statistical variation of the measured dose. In addition, a wide range of neutron energies is produced by a high-energy linear accelerator associated with a wide range of radiation weighting factors (approximately 5 – 20) thus causing an inevitable difficulty in measuring neutron dose equivalent. Despite these variations, the measurement results were generally in agreement with the reported values. In Chapter 7, the use of these TLDs in determination of peripheral doses in Rando phantom will be presented and the degree of variations in the estimated second primary cancer risks associated with variations in the measured peripheral doses from the TLD measurements will be investigated.

At all measuring points, the contribution of thermal neutrons to total dose equivalent was much less than that of fast neutrons. Using a Bonner sphere system

based on passive gold activation detector to measure neutron doses produced from 18 MV Varian 2100C linear accelerator, it has been observed that the dose equivalent rate (mSv/h) at 1 m from the isocentre consisted from contribution from thermal, intermediate, and fast neutrons as 1.4%, 7.8%, and 90.8%, respectively (Fernandez *et al* 2007). Thermal neutron dose equivalents measured in this current work were also small. At 1 meter from the isocentre thermal neutrons contributed up to around 3.0% of the total neutron dose.

6.6 Conclusion

In this chapter, it has been demonstrated that ^{7}LiF:Mg,Cu,P and ^{6}LiF:Mg,Cu,P glass-rod TLDs in pairs can be used for measurements of photon and neutron doses in a mixed-radiation field produced by medical linear accelerators operating at high accelerating potential. The ^{7}LiF:Mg,Cu,P glass-rod TLDs can be calibrated using the linear accelerator to identify their radiation sensitivity and linearity. Without standard neutron sources, calibration of ^{6}LiF:Mg,Cu,P TLDs may be done with a high-energy linear accelerator. However, a calibrated neutron dosimeter such as CR-39 etch-track or bubble detectors is needed to cross-calibrate and to obtain relative readout-to-dose conversion factor.